Biophysical Journal
Article

Biophysical Society

Single Proteoliposome High-Content Analysis Reveals Differences in the Homo-Oligomerization of GPCRs

Samuel M. Walsh,[1] Signe Mathiasen,[1] Sune M. Christensen,[1] Jonathan F. Fay,[2] Christopher King,[3] Davide Provasi,[4] Ernesto Borrero,[4] Søren G. F. Rasmussen,[5] Juan Jose Fung,[6] Marta Filizola,[4] Kalina Hristova,[3] Brian Kobilka,[6] David L. Farrens,[7] and Dimitrios Stamou[1,*]

[1]Bionanotechnology and Nanomedicine Laboratory, Department of Chemistry, University of Copenhagen, Copenhagen, Denmark; [2]Department of Biochemistry and Biophysics, University of North Carolina Medical School, Chapel Hill, North Carolina; [3]Program in Molecular Biophysics, Johns Hopkins University, Baltimore, Maryland; [4]Department of Pharmacological Sciences, Icahn School of Medicine at Mount Sinai, New York, New York; [5]Department of Neuroscience and Pharmacology, University of Copenhagen, Copenhagen, Denmark; [6]Department of Molecular and Cellular Physiology, Stanford University School of Medicine, Palo Alto, California; and [7]Department of Biochemistry and Molecular Biology, Oregon Health and Science University, Portland, Oregon

ABSTRACT G-protein-coupled receptors (GPCRs) control vital cellular signaling pathways. GPCR oligomerization is proposed to increase signaling diversity. However, many reports have arrived at disparate conclusions regarding the existence, stability, and stoichiometry of GPCR oligomers, partly because of cellular complexity and ensemble averaging of intrareconstitution heterogeneities that complicate the interpretation of oligomerization data. To overcome these limitations, we exploited fluorescence-microscopy-based high-content analysis of single proteoliposomes. This allowed multidimensional quantification of intrinsic monomer-monomer interactions of three class A GPCRs (β_2-adrenergic receptor, cannabinoid receptor type 1, and opsin). Using a billion-fold less protein than conventional assays, we quantified oligomer stoichiometries, association constants, and the influence of two ligands and membrane curvature on oligomerization, revealing key similarities and differences for three GPCRs with decidedly different physiological functions. The assays introduced here will assist with the quantitative experimental observation of oligomerization for transmembrane proteins in general.

INTRODUCTION

G-protein-coupled receptors (GPCRs) comprise the most abundant family of transmembrane proteins (TMPs) in mammalian cells (1,2); they control multiple signaling transduction pathways and effect crucial physiological reactions in response to a plethora of endo- and exogenic stimuli (1). Historically, GPCRs were considered monomeric entities, but multiple recent studies indicate that they frequently exist as dimeric or oligomeric assemblies (3). Oligomerization is proposed to increase pharmacological diversity by stabilizing alternative receptor conformations (4) and thereby promoting alternative signaling pathways (5). Thus, a concerted effort has gone into understanding GPCR oligomerization (3). However, many reports have arrived at disparate conclusions regarding the existence, stability, and stoichiometry as well as the influence of endogenous and pharmacological ligands on GPCR oligomers (5–8).

The majority of GPCR oligomerization studies have been performed in living cells using optical resonance energy transfer (RET) methods to interrogate an ensemble of receptors (see Table 1 from Kasai and Kusumi (9)) or, more lately, single receptor molecules (6). However, cellular complexity, although establishing biological relevance (8), makes it difficult to disentangle the association properties intrinsic to direct receptor monomer-monomer interactions from the influence of multiple effectors that have been shown to impact oligomerization, including confining cytoskeletal elements (10), lipid rafts (11), interacting proteins (12), or extracellular contacts (13). To provide an analysis of GPCR oligomerization unbiased by cellular complexity, we purified and reconstituted GPCRs in proteoliposomes.

Proteoliposomes are model systems that are in principle particularly well adapted to studies of oligomerization because their continuous spherical surface allows TMPs to

Submitted January 16, 2018, and accepted for publication May 31, 2018.

*Correspondence: stamou@nano.ku.dk

Samuel M. Walsh and Signe Mathiasen contributed equally to this work.

Editor: Charles Deber.

https://doi.org/10.1016/j.bpj.2018.05.036

diffuse perpetually within the plane of the lipid bilayer and oligomerize without any hindrance imposed by physical barriers. However, the reproducible production of homogenous proteoliposomes is a great challenge in proteoliposome reconstitution (14–19). A recent study demonstrated that individual proteoliposomes within a reconstitution have a highly heterogeneous protein-to-lipid (P/L) ratio that severely skews ensemble measurements of oligomerization (20). In general, heterogeneities are observed for different samples independent of protein type or reconstitution method (14–20). To overcome this limitation, we exploited fluorescence-microscopy-based high-content analysis (HCA) of single nanoscale proteoliposomes (20). This allowed the accurate multidimensional quantification of pure monomer-monomer interactions unbiased by cellular complexity and intrareconstitution heterogeneities.

Our data provide quantitative comparative insight into the oligomerization of three class A GPCRs: the β_2-adrenergic receptor (β_2AR), which binds adrenaline and noradrenaline in a variety of tissues to stimulate smooth muscle cell contraction (1); the cannabinoid receptor type 1 (CB_1), which binds endocannabinoids in neurons and plays a role in memory, learning, and addiction (21); and opsin, the non-ligand-bound rhodopsin that mediates visual phototransduction in retinal cells (22). To characterize the oligomerization process in-depth, we quantified the number of protein monomers that associate per cluster (stoichiometry), the strength of monomer association (equilibrium constant and related association energy), and the influence of selected ligands and of the geometric structure of the surrounding lipid bilayer. This enabled us to identify key similarities and differences among the three GPCRs with decidedly different physiological functions.

MATERIALS AND METHODS

Cloning, receptor purification, and labeling

Quantitative fluorescence RET (FRET) microscopy requires that each receptor carry a single fluorescent label; furthermore, to make direct comparisons between GPCRs, the fluorescent labeling site must be placed on the same region as the receptors. We therefore engineered receptor constructs with a specific cysteine labeling site for fluorescent labeling on the surface-exposed part of helix 8 (see Supporting Materials and Methods, Receptor Constructs). For all receptors used in this study, it was confirmed that the single reactive cysteine mutant was functional using ligand binding assays (for details, see β_2AR (23), CB_1 (24), and opsin (25)), and that fluorescent labeling did not impair functionality. Expression, purification, and fluorescent labeling with either Cy3- or Cy5-maleimide (Amersham Biosciences, Little Chalfont, UK) was carried out as previously described (β_2AR (23), CB_1 (26), opsin (27)).

Proteoliposome preparation

Fluorescently labeled receptors were reconstituted into proteoliposomes with a total protein to lipid ratio of 1:1000. Oregon Green 1,2-dihexadecanoyl-sn-glycero-3-phosphoethanolamine (OG-DHPE) was included at 0.1 mol percentage to fluorescently label all proteoliposomes, and 1,2-distearoyl-sn-glycero-3-phosphoethanolamine-poly(ethylene glycol)$_{2000}$-biotin (DSPE-PEG$_{2000}$-biotin) was included at 0.1 mol percentage to enable tethering to the passivated microscopy glass surface (see Fluorescence Microscopy). To make direct comparisons between different GPCRs, the receptors were reconstituted into the simplest lipid composition required to maintain receptor functionality (see below). Four different proteoliposome preparations were produced for each receptor: 1) both GPCR-Cy3 and GPCR-Cy5 reconstituted at a 1:1 ratio for quantification of FRET, 2) empty liposomes with no receptors reconstituted, 3) only GPCR-Cy3 reconstituted, and 4) only GPCR-Cy5 reconstituted. Samples 2–4 were prepared as controls to carefully quantify possible intensity signal contaminations in the various microscopy detection channels used in this study (see Quantification of E_{FRET}).

Proteoliposomes were prepared as previously described (20). Briefly, β_2AR proteoliposomes were prepared by resuspending a dried lipid film of 1,2-dioleoyl-sn-glycero-3-phosphocholine/cholesteryl hemisuccinate/1,2-dioleoyl-sn-glycero-3-phosphoglycerol/OG-DHPE/DSPE-PEG$_{2000}$-biotin (79.4:10:10:0.5:0.1) (Avanti Polar Lipids, Alabaster, AL; Steraloids, Newport, RI; Invitrogen, Carlsbad, CA) in buffer (20 mM HEPES, 100 mM NaCl, 1% octylglucoside (pH 7.5)) (20). The lipid detergent mixture was sonicated for 1 h on ice, and subsequently, receptors were added in the desired lipid to protein ratio. After incubation on ice for 2 h, proteoliposomes were formed by the removal of detergent on a Sephadex G-50 (fine) column (25 × 0.8 cm) (Sigma Aldrich, St. Louis, MO).

CB_1 and opsin proteoliposomes (28) were prepared by mixing labeled receptor, solubilized in 0.05% *n*-dodecyl-β-$_D$-maltoside, and lipids 1-palmitoyl-2-oleoyl-sn-glycero-3-phosphocholine/1-palmitoyl-2-oleoyl-sn-glycero-3-phosphoglycerol/OG-DHPE/DSPE-PEG$_{2000}$-biotin (59.85:39.85:0.2:0.1) (Avanti Polar Lipids, Steraloids, Invitrogen), solubilized in 0.5 M sodium cholate with approximately two-thirds vol of Bio-Beads SM-2 (Bio-Rad, Hercules, CA) overnight at 4°C. The Bio-Beads were removed by centrifugation (1000 × *g*, 1 min), yielding proteoliposome preparations in 20 mM HEPES (pH 7.3), 150 mM NaCl, 2 mM $MgCl_2$, and 1 mM EDTA. Both Bio-Beads and size exclusion chromatography are robust methods for removing detergents. Once proteoliposomes are diluted to 0.0025 g/L and added to the glass surface for microscopy imaging (see section below), any remaining detergent will have had ample opportunity to dissociate into the assay buffer before the actual microscopy measurement takes place. We therefore evaluate the likelihood for any trace amounts of leftover detergents to be negligible and not influence the dimerization studies. Also, no lipidomic studies were carried out after reconstitution, as we anticipated the bulk lipids present would comprise the large excess of reconstitution lipids, either 1,2-dioleoyl-sn-glycero-3-phosphocholine/cholesteryl hemisuccinate/1,2-dioleoyl-sn-glycero-3-phosphoglycerol for β_2AR or 1-palmitoyl-2-oleoyl-sn-glycero-3-phosphocholine/1-palmitoyl-2-oleoyl-sn-glycero-3-phosphoglycerol for opsin and CB_1.

Fluorescence microscopy

We immobilized the biotinylated proteoliposomes on a poly-L-lysine (PLL)-graft-PEG/PLL-graft-PEG-biotin passivated microscopy glass surface in homebuilt microscope chambers through NeutrAvidin, as described previously (20). Chamber parts were cleaned extensively using ethanol and Milli-Q water. Glass slides (thickness 170 ± 10 μm) were cleaned by consecutive rounds of sonication by 2% (v/v) Helmanex, following 3 × Milli-Q water and 2 × methanol. Glass slides were dried in nitrogen flow, plasma etched for 2 min, mounted in a microscope chamber, and incubated with a mixture of 1000:6 PLL-g-PEG and PLL-g-PEG-biotin (19; SuSoS AG, Dübendorf, Switzerland) (1 g/L) in surface buffer (15 mM HEPES (pH 5.6)) for 30 min. After carefully washing with sample buffer (β_2AR: 20 mM HEPES, 100 mM NaCl (pH 7.5); CB_1 and opsin: 20 mM HEPES, 100 mM NaCl, 2 mM $MgCl_2$, 1 mM EDTA (pH 7.5)), the surfaces were incubated with 0.1 g/L NeutrAvidin in surface buffer for 10 min, after additional washing 10 × with sample buffer. We controlled proteoliposome

surface density by adding samples at a low concentration (0.0025 g/L) to achieve spatial separation between particles and then washed the chamber 10 × with sample buffer. Proteoliposomes were imaged in sample buffer with a Leica TCS-SP5 inverted confocal microscope (Leica, Wetzlar, Germany) and an oil immersion objective HCX PL APO CS × 100 (NA 1.4). 476, 543, and 633 nm laser lines were used to excite the OG-DHPE, Cy3, and Cy5 fluorophores, respectively. The OG intensity signal was filtered out in the range of 486–539 nm and collected by a photomultiplier tube. Cy3 and Cy5 emissions were detected by avalanche photodiodes (APDs) with the emission signals cut off at 625 nm between APD1 and APD2 using a dichroic mirror BS625 (Chroma Technology, Bellows Falls, VT). Cy3 and Cy5 emissions were filtered by bandpass filters BrightLine HC 585/40 (Semrock, Rochester, NY) and HQ675/55M (Chroma Technology), respectively. Images had a resolution of 1024 × 1024 pixels, with a pixel size of 50.5 nm sample length and a bit depth of 16 and were acquired with a scan speed of 400 Hz. All fluorescence microscopy was carried out at room temperature.

Single fluorescent particle characterization

Automated detection and fitting of single fluorescent particles was carried out using software written in Igor Pro v. 6.01 (WaveMetrics, Portland, OR), as previously described (20). Briefly, a two-dimensional Gaussian bell was fitted to each diffraction-limited intensity to assign an *xy* center and measure the integrated fluorescence intensity. A circularity cutoff of 0.5 (minor axis divided by major axis) was applied to reject spurious intensity signals. Colocalization was defined as particles in separate color channels having centers within a distance of three pixels.

Quantification of E_{FRET}

To accurately determine the efficiency of energy transfer (E_{FRET}), fluorescent signals must be carefully corrected for several signal contaminations. We used three control samples (preparations 2–4 described in Proteoliposome Preparation) and imaged them, employing the exact same microscopy conditions as for the proteoliposomes investigated for FRET (preparation 1). Imaging the single-labeled proteoliposomes allowed us to measure the amount of fluorescence intensity leaking into neighboring emission detection channels (emission bleed-through) and also the amount of unintended fluorescence intensity resulting from excitation by neighboring laser lines (indirect excitation). We identified three such fluorescent signal contaminations and were able to accurately determine E_{FRET} by using the correction factors (ω, α, β) (see Supporting Materials and Methods, Determining Fluorescent Signal Correction Factors (ω, α, β)). In the following section superscript, ^{0} denotes raw uncorrected intensities. I_D and $I_A^{0,FRET}$ are the donor and acceptor intensities excited by the donor laser line (543 nm).

The GPCR-Cy3 emission (I_D^0) was corrected for OG-DHPE bleed-through (ω) using Eq. 1:

$$I_D = I_D^0 - \omega I_M^0. \tag{1}$$

The FRET ($I_A^{0,FRET}$) emission was corrected for two signal contaminations—Cy3 emission bleeding into the acceptor detection channel (β) and the indirect excitation of Cy5 with the donor laser (543 nm) (α)—using Eq. 2:

$$I_A^{FRET} = I_A^{0,FRET} - \beta I_D - \alpha I_A^0. \tag{2}$$

E_{FRET} was finally calculated according to Eq. 3 (29):

$$E_{FRET} = \frac{I_A^{FRET}}{I_A^{FRET} - \gamma I_D}, \tag{3}$$

where

$$\gamma = \frac{\Phi_A \eta_A}{\Phi_D \eta_D} \tag{4}$$

was introduced to decouple E_{FRET} from instrumental and photophysical (30) effects. (Φ_A/Φ_D) corrected for differences in detection efficiencies (η_A/η_D) and differences in quantum yields of the Cy3 and Cy5 fluorophores. (Φ_A/Φ_D) and (η_A/η_D) were determined as carried out previously (20).

RESULTS

Direct imaging of single proteoliposomes enables HCA of compositional heterogeneities

We reconstituted fluorescently labeled GPCRs in proteoliposomes doped with a lipid-coupled dye and produced arrays of single surface-tethered proteoliposomes that could be imaged individually with fluorescence microscopy (Fig. 1 *A*). We have previously measured nanoscale liposomes at the single particle level and demonstrated that surface immobilization did not compromise either the spherical or the physiochemical integrity of the particles (31,32). By using single proteoliposomes, we reduced the amount of receptor needed for each assay to ~6 pg, a 10^9-fold reduction over traditional assays (see Supporting Materials and Methods, Total Receptor Per Assay). Labeling of both proteins and the membrane phase allowed us to accurately quantify the amount of GPCRs and lipids per proteoliposome and concurrently measure oligomerization by FRET (20).

We site-specifically labeled previously well-characterized and functionally active GPCR mutants with either Cy3 or Cy5 fluorophores at single reactive cysteines on the solvent-exposed helix 8 region of each receptor. Receptors were reconstituted in proteoliposomes using standard protocols of gel chromatography and removal of detergent using Bio-Beads (Materials and Methods). Mixing receptors labeled with Cy3 (donor, D) and Cy5 (acceptor, A) allowed us to quantify GPCR homo-oligomerization as the E_{FRET} between D- and A-labeled receptors within single nanoscale proteoliposomes.

Fluorescent confocal microscopy enabled the parallel collection of fluorescent intensities from thousands of individual proteoliposomes (Fig. 1 *B*). We recorded four intensity signals per proteoliposome—lipid dye, D, A, and FRET (A emission at D excitation) (Fig. 1, *B* and *C*)—and extracted the position and integrated intensity for all four signals by fitting a two-dimensional Gaussian function.

Labeling of the proteoliposome lipid phase permitted the discrimination of receptors reconstituted in proteoliposomes from protein aggregates as well as empty liposomes by identifying particles with coexisting lipid and receptor intensities. This approach allowed us to then separate the proteoliposome fraction into the relevant subpopulation

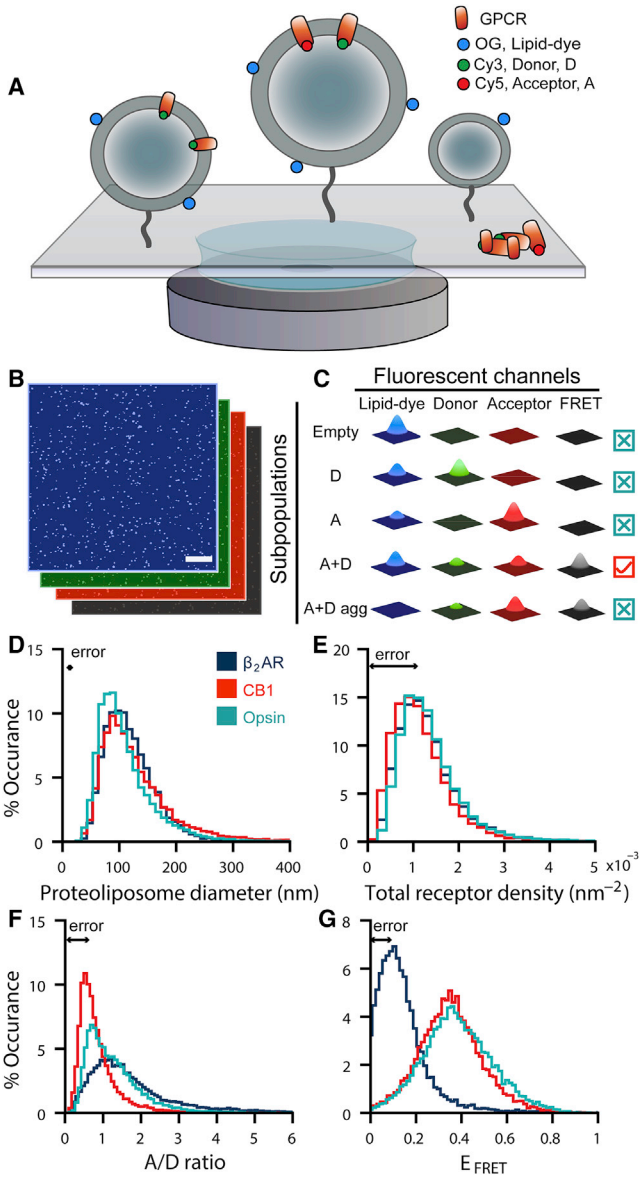

FIGURE 1 Single proteoliposome high content analysis allows identification of intrareconstitution compositional heterogeneities. (*A*) Single proteoliposomes are tethered to a functionalized microscopy glass surface at dilute densities to ensure spatially separated particles. Proteoliposome membranes are labeled with a lipid-coupled dye Oregon Green DHPE (membrane, OG), and reconstituted GPCRs are labeled with either Cy3 (Donor, D) or Cy5 (Acceptor, A) fluorophores. (*B*) Typical confocal image micrographs of single proteoliposomes are shown. Scale bars, 10 μm. Micrographs are recorded for four fluorescent intensity signals: OG (*blue*), Cy3 (*green*), Cy5 (*red*), and FRET (*black*). (*C*) Colocalization of four unique intensity signals per proteoliposome reveals a subset of different particles within a reconstitution sample, namely proteoliposomes without reconstituted GPCRs (Empty), proteoliposomes harboring only donor-labeled or only acceptor-labeled GPCRs (D or A), proteoliposomes harboring both donor-labeled and acceptor-labeled GPCRs (A+D), and protein aggregates (A+D agg). (*D–F*) Histograms display individual proteoliposome (*D*) diameters, (*E*) receptor densities, (*F*) A/D ratios, and (*G*) FRET efficiencies (E_{FRET}). Histograms of β_2AR and opsin receptor densities overlay one another in (*E*). For each GPCR, data comprise $n >$ 12,800 single proteoliposomes from >5 technical replicates. Errors shown in (*D*)–(*G*) represent the full width of histograms composed from single proteoliposome errors for each parameter. Solely in this figure, data for β_2AR are reproduced from (20) to facilitate a direct comparison to CB_1 and opsin.

for FRET studies containing both D- and A-labeled GPCRs (A+D, Fig. 1 *C*, *red box*) from the unwanted populations of singly labeled proteoliposomes. Our colocalization analyses revealed that each receptor reconstitution contained subpopulations with highly different GPCR compositions and that a significant number of particles in each reconstitution were unusable for FRET studies (Fig. S2 *A*). We selected the relevant proteoliposomes (A+D) from the total population of particles for oligomerization studies: 56 ± 2% for β_2AR, 22 ± 2% for CB_1, and 18 ± 3% for opsin. Although the mechanisms behind these differences in receptor reconstitution remain unknown, our single-particle approach allows us to isolate this population across different reconstitution samples.

We then quantified intrasample heterogeneities within the selected proteoliposome population. GPCR oligomerization is strongly dependent on receptor concentration; we therefore carefully determined the receptor concentration of each single proteoliposome by quantifying the surface area using a previously published calibration procedure and the absolute number of receptors employing single-molecule photobleaching (see Supporting Materials and Methods, Proteoliposome Size and Receptor Density). We observed proteoliposome diameters from 40 to 400 nm (Fig. 1 *D*) and absolute receptor surface densities covering a broad range of $\sim 0.3 - 3.0 \times 10^{-3}$ receptors/nm^2 (Fig. 1 *E*). Each proteoliposome contained between $\sim$10 and 200 receptors (Fig. S2 *B*) with an average of 50 receptors per proteoliposome. Analysis of single proteoliposomes also revealed a broad distribution of A/D ratios (Fig. 1 *F*) spanning from 0.2 to 5.0 within a single reconstitution sample prepared with a nominal mixing-ratio of 1:1. We propagated the single proteoliposome errors for each parameter in Fig. 1, *D–G* from the uncertainty associated with quantifying the fluorescence intensity signals from GPCRs and lipids and plotted them as histograms (see Supporting Materials and Methods, Error Propagation). The variation in compositional heterogeneities substantially exceeded the full width of the error histograms (Fig. 1, *D–F*, *black arrows*), demonstrating that the variations in diameter (more than 47-fold larger than errors), density (more than fivefold larger than errors), and A/D ratios (more than sixfold larger than errors) can be used for HCA.

Oligomer-specific FRET allows quantification of GPCR oligomerization

FRET association studies require careful controls to verify that the energy transfer signal is specific to physical interactions between receptors. The homogeneous orientation of the receptor in the membrane is crucial

to prevent non-natural top-to-tail oligomerization events. We therefore verified that our proteoliposome preparations contained a uniform receptor orientation (β_2AR ~90% outside out (23) and CB_1 and opsin >95% inside out) (see Fig. S1 and Supporting Materials and Methods, Orientation of Receptors). Additionally, to avoid measuring artificial receptor crowding, the average distance between receptors must be considerably larger than the Förster radius for the D and A fluorophores. Our calculations reveal that average monomer distances (assuming noninteracting monomers) at the observed high- and low-density extremes (Fig. 1 *E*) were respectively three- and ninefold larger than the ~5.6 nm Cy3/Cy5-Förster radius, demonstrating that protein crowding does not contribute substantially to the FRET readout (see Supporting Materials and Methods, Average Monomer Distance).

To demonstrate that we observed specific oligomerization and rule out that E_{FRET} is not contaminated significantly by random collisions of receptors, we have previously used a theoretical scheme showing that E_{FRET} always exceeded the expected E_{FRET} from random encounters (20). Here, we followed the improved experimental guidelines of Lambert and colleagues, who recently used extensive controls to show that RET between noninteracting proteins may only increase as a function of acceptor density, whereas RET resulting from specific association should also be sensitive to donor density (33). To run this test, we plotted E_{FRET} as a function of A density at a low and high D density, respectively (Fig. S2, *C–H*). We found a relative increase in E_{FRET} at lower D, indicating that E_{FRET} was sensitive to D density. Thus, these results confirmed that E_{FRET} was not influenced by random collisions of receptors in the density ranges investigated here and that all three GPCRs investigated engaged in specific oligomerization.

Having ruled out the contribution of top-to-tail dimerization, receptor crowding, and random collisions, we could now interpret E_{FRET} measurements from more than 12,000 individual proteoliposomes for each receptor. We observed a wide distribution of E_{FRET} (Fig. 1 *G*) (more than 17-fold larger than errors) as a consequence of the large spread A/D ratios (Fig. 1 *F*) and protein densities (Fig. 1 *E*). Interestingly, the CB_1 and opsin E_{FRET} peak positions, 0.34 ± 0.001 and 0.37 ± 0.001, respectively, were shifted to higher efficiencies than for the β_2AR, 0.13 ± 0.001. These results indicate that the oligomerization of CB_1 and opsin differs markedly from that of β_2AR because of differences in both association stoichiometry and energy, as we demonstrate further on.

Ensemble-average proteoliposome measurements can severely bias oligomerization assays

Typically, ensemble association studies estimate the average P/L ratio of proteoliposomes from the starting material of reconstitution samples and measure TMP oligomerization with ensemble RET. Having first identified that a significant number of particles were not the relevant A+D proteoliposomes (Fig. 1 *C*; Fig. S2 *A*), we next evaluated if an ensemble-average from this sample represented the single proteoliposome distributions of densities, A/D ratios, and E_{FRET} (Fig. 1, *E–G*). We determined the percentage of single proteoliposomes having values within a 10% error margin around the predicted ensemble-average. We based the 10% error margin on previous reports of RET oligomerization measurements of GPCRs in proteoliposomes (23) and live cells (34).

We calculated a bulk receptor density (ρ_{bulk}) under the assumption that all lipid and receptor materials were used to produce proteoliposomes (Table S1). For all three receptors, ρ_{bulk} ($1.7 \pm 0.2 \times 10^{-3}$ receptors/nm^2) represented less than 15% of the single proteoliposomes (Fig. S2 *I*). Additionally, even though proteoliposomes were prepared at a nominal 1:1 A/D ratio, only 10–12% of single proteoliposomes had an A/D ratio within 10% of the intended A/D = 1 (Fig. S2 *I*; Table S1). Both observations demonstrate that the common assumption permitting protein density and A/D ratios to be estimated from the amount of starting materials must be used with great caution.

Finally, we estimated an ensemble E_{FRET} average (see Supporting Materials and Methods, Ensemble Proteoliposome E_{FRET}) including signals from A+D proteoliposomes, protein aggregates, and proteoliposomes carrying only D- or A-labeled GPCRs (Fig. S2 *I*; Table S1). The calculated ensemble $E_{FRET\text{-}bulk}$ was similar for all three receptors (β_2AR 0.27, CB_1 0.27, and opsin 0.22) but deviated greatly from the single proteoliposome E_{FRET} peak positions (see Fig. 1 *G*) and would incorrectly suggest that the three GPCRs had similar oligomerization behavior. In addition, only 4% (β_2AR), 14% (CB_1), or 7% (opsin) of single proteoliposomes were within 10% of the predicted $E_{FRET\text{-}bulk}$ (Fig. S2 *I*; Table S1). These calculations demonstrate that protein aggregates and proteoliposomes carrying only D- or A-labeled GPCRs severely alter ensemble-averaged E_{FRET} signals. In contrast to the convoluted and biased ensemble values, single-proteoliposome measurements revealed important differences in the oligomerization propensity of the β_2AR, CB_1, and opsin.

Identifying unique apparent stoichiometry and association modes for three class A GPCRs

We have previously shown that compositional heterogeneities can be exploited to perform HCA as a function of TMP density and A/D ratio to extract quantitative parameters of oligomerization (20). Here, we went on to quantify both the stoichiometry and association energies for β_2AR, CB_1, and opsin.

The ratio of D- and A-labeled GPCRs in an oligomer can be used to determine the apparent average oligomer

stoichiometry (23,34–38). In the simple case of a D-A dimer, the amount of energy transferred by the D- to the A-fluorophore is dependent on the proximity of the two fluorophores (39). In higher-order oligomers, where for example a D-fluorophore may excite multiple acceptors, the A/D ratio will also affect E_{FRET}. To determine the stoichiometry of each GPCR, we used the widely applied method of Veatch and Stryer (38) to relate E_{FRET} to the A/D ratio and extract the apparent average oligomer stoichiometry as a fitting parameter (Fig. 2 *A* and Supporting Materials and Methods, Receptor Stoichiometry). The Veatch and Stryer theory has been a well-established approach that allows the direct comparison of receptors with stoichiometries greater than dimers; progress is currently being made in the field to improve this classical theory (40).

We determined the apparent average stoichiometry for each receptor by fitting this theoretical scheme to all proteoliposomes ($n > 12{,}800$) presented in Fig. 1, *D–G*. The stoichiometry analysis reveals interesting differences between the three receptors. We find that the β_2AR forms oligomers of much lower order than CB_1 or opsin (Fig. 2 *A*) with their apparent average stoichiometries being 1.8 ± 0.2, 4.9 ± 0.1, and 4.1 ± 0.2, respectively. Taken together, our results in a simple lipid system reveal that β_2AR, CB_1, and opsin each have a unique propensity to form oligomers of a certain stoichiometry when oligomerization is solely governed by receptor-receptor interactions.

The direct comparison of our findings with the literature is not straightforward. GPCR oligomerization has been largely measured with ensemble-based RET studies in living cells that have not necessarily arrived at a consensus with respect to individual receptor oligomerization or stoichiometries (7). Given the disparity of information in the literature, it is hard to make a direct comparison between live cell studies and single proteoliposome studies; however, we would like to note that there is existing support in live cells that β_2AR can form a dimer (34,41,42) and that the smallest repeating unit of rhodopsin in isolated disk membranes is tetrameric (43–45).

We then proceeded to quantify the association energies of oligomerization. We previously applied the method of Wolber and Hudson (46) to determine the apparent Gibbs free energy of association for β_2AR; however, this methodology is restricted to a dimer system and did not satisfyingly fit the CB_1 and opsin data. We therefore built upon the advanced kinetic theory of FRET by Raicu (47,48) and computed the theoretical apparent FRET efficiency as a function of total concentration for two models of a monomer-dimer (β_2AR) and monomer-tetramer (CB_1 and opsin) reaction (see Supporting Materials and Methods, Receptor Association Energies). To exclude any possible contribution of membrane curvature on protein diffusion (49) and thus oligomerization, we selected proteoliposomes within an extremely narrow diameter range (120–130 nm). We then fitted the ratio of oligomers to free monomers (oligomeric fraction) as a function of total receptor density to the binding curves for each oligomer association model and extracted the association constant of oligomerization K_a.

We determined the apparent Gibbs free energy of association for β_2AR, -3.9 ± 0.007 kcal/mole (which is comparable to that found using the classical Wolber and Hudson method, -4.7 ± 0.2 kcal/mole (20)) and for CB_1, -15.2 ± 0.8 kcal/mole. The CB_1 association was stronger than that of the β_2AR, as expected by comparison of the oligomeric fractions of the two receptors in Fig. 2 *B* (i.e., at 0.6×10^{-3} receptors/nm^2, ~40% of β_2AR is oligomeric, whereas ~75% of CB_1 is oligomeric). We could not accurately fit the data for opsin with our association model because the oligomeric fraction of the receptor did not vary substantially within the range of receptor densities

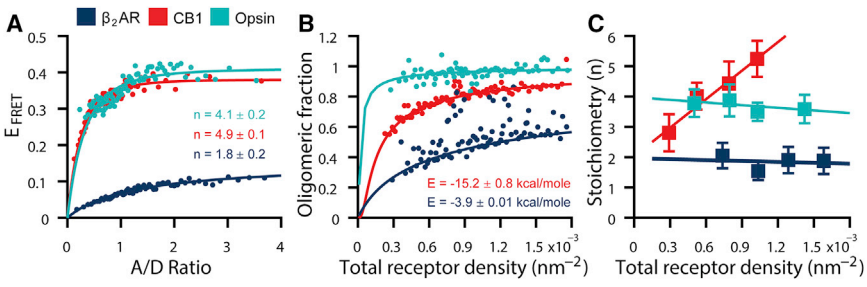

FIGURE 2 Quantification of GPCR association strengths and stoichiometry. (*A*) To quantify the apparent average stoichiometry of each receptor, E_{FRET} is evaluated as a function of A/D ratios and fit with Eq. S3. From the fit, we extract the apparent average stoichiometry (n). The data shown in (*A*) comprise >12,400 single proteoliposomes. For clear visualization, E_{FRET} values of single proteoliposomes are binned (200 single proteoliposomes per bin), and a weighted average of each bin is displayed. Uncertainties are less than or equal to displayed marker size. (*B*) To determine the association energies of oligomerization (E), the GPCR oligomeric fraction is evaluated as a function of total receptor density, and data are fitted based on a monomer-dimer (β_2AR) or monomer-tetramer (CB_1 and opsin) thermodynamic equilibrium using the kinetic theory of FRET (Supporting Materials and Methods). We determine the association energies for β_2AR (-3.9 ± 0.007 kcal/mole) and CB_1 (-15.2 ± 0.8 kcal/mole) and find that opsin is a high-affinity oligomer. In (*B*), data were binned (10 proteoliposomes per bin), and a weighted average is shown. For each GPCR, a total of $n > 820$ single proteoliposomes was included in the analysis. (*C*) GPCR stoichiometry is shown as a function of total receptor density. Fitting and extracting the apparent average stoichiometry was repeated as in (*A*) for four proteoliposomes selections with increasing receptor densities while maintaining a constant proteoliposome diameter within ±15 nm of the mean (see Table S1). The apparent average stoichiometry from each density selection is shown. For each GPCR, data comprise $n > 2500$ single proteoliposomes, where uncertainties represent ±1 SD calculated from the fit of Eq. S3. A linear fit to each data set is included to guide the eye. Our analysis reveals a unique stoichiometry and association mode for each GPCR.

that we could measure (Fig. 2 *B*), indicating that opsin oligomerizes at much lower densities than CB_1 or β_2AR.

Increasing receptor density has been proposed to shift the equilibrium from monomers to oligomers because of the higher number of protein-protein encounters (42). Thus, one would expect the apparent stoichiometry to increase on average with protein density. The multidimensional heterogeneity of our samples allowed us to test this hypothesis because we were able to quantify E_{FRET} as a function of A/D ratio for multiple receptor densities. In Fig. 2 *C*, we plot the apparent average GPCR oligomer stoichiometry for four groups of proteoliposomes with increasing surface densities while maintaining a constant proteoliposome diameter. The average apparent stoichiometry of CB_1 increased as expected. Interestingly, within the limits of statistical uncertainty, we did not observe a similar change for β_2AR (Fig. 2 *B*). The apparent stoichiometry of opsin was constant over these receptor densities, which was not surprising given the constant oligomeric fraction (Fig. 2 *B*) of opsin within this range of densities.

Membrane curvature modulates GPCR oligomerization

Upon ligand binding, GPCRs are thought to desensitize by internalization into endocompartments of high membrane curvature (50). However, high membrane curvature has recently attracted considerable attention for being able to regulate multiple biophysical properties of TMPs (49,51–53). We therefore set out to explore whether GPCR oligomerization is sensitive to changes in the local membrane shape surrounding the receptor. We did this by evaluating E_{FRET} as a function of liposome diameter (Fig. 3 *A*).

Our measurements revealed a pronounced effect on E_{FRET}, changing from ~0.05 in a highly curved membrane (50 nm in diameter) to ~0.12 in a more planar membrane (300 nm in diameter) for β_2AR (Fig. 3 *A*). Over the same range of curvatures, E_{FRET} changed from ~0.30 to 0.40 for both CB_1 and opsin (Fig. S3, *B* and *C*). These observations suggest that highly bent bilayers reduce the propensity of GPCRs to oligomerize.

To exclude any convolution of the curvature effect with variations in protein density and A/D ratio, we selected proteoliposomes with a constant range of acceptor and donor densities for this analysis (Fig. S3, *D–F*). Ensuring that both acceptor and donor densities are constant, we can ascribe the observed perturbation in E_{FRET} to solely originate from the influence of membrane curvature. Interestingly, we also found that the apparent stoichiometry of β_2AR, CB_1, and opsin decreased with high membrane curvature (Fig. 3 *B*; Fig. S4). Thus, our data reveal that high membrane curvature can destabilize both the propensity of GPCRs to oligomerize and the size of the oligomers.

A major challenge in the membrane curvature field is to design experimental approaches for controlling and measuring the effect of both positive and negative curvature on TMP function (54). Our assay provided an unambiguous assessment of both types of membrane bends on GPCR oligomerization because the receptors favored uniform and different orientations in the proteoliposomes (β_2AR, outside out, and CB_1 and opsin, inside out). We found that high

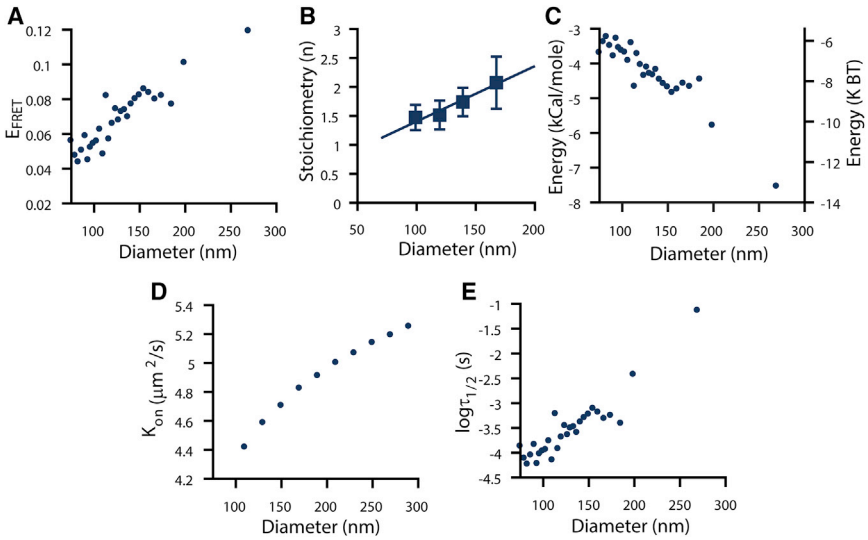

FIGURE 3 Membrane curvature modulates GPCR oligomerization. (*A*) β_2AR E_{FRET} is shown as a function of proteoliposome diameter. E_{FRET} increases as proteoliposome diameter increases, and membrane curvature decreases. Data in (*A*) have a constant receptor density and A/D ratio (Fig. S3). Corresponding data for CB_1 and opsin are shown in Fig. S3. In (*A*), data were binned (75 single proteoliposomes per bin), and a weighted average is shown. Data in (*A*) comprise a total of $n = 2175$ single proteoliposomes with uncertainties less than or equal to the displayed marker size. (*B*) Increasing membrane curvature decreases oligomer stoichiometry. Stoichiometry analysis was repeated as in Fig. 2 *A* for proteoliposome selections with increasing diameters while maintaining a constant receptor density within $\pm 0.2 \times 10^{-3}$ receptors/nm^2 of the mean (see Table S1). Corresponding data for CB_1 and opsin are shown in Fig. S4. The apparent average stoichiometry from each diameter selection is shown. Data in (*B*) comprise $n > 2500$ single proteoliposomes, where uncertainties represent ± 1 SD calculated from the fit of Eq. S3. A linear fit to the data set is included to aid interpretation. (*C*) Standard Gibbs free β_2AR association energy is shown as a function of liposome diameter and membrane curvature. β_2AR association energy is decreased by ~4 kcal/mole from −3.8 to −7.8 kcal/mole in extremely curved versus quasi-planar membrane geometries. (*D*) Dimerization on-rates (k_{on}) (μm^2/s) are shown as a function of liposome diameter. (*E*) Dimer lifetimes are calculated for the proteoliposome selection of (*C*). High membrane curvature decreases GPCR oligomerization as well as dimerization on-rates and lifetimes.

membrane curvature restrains receptor interactions for both positive (β_2AR, outside out) and negative membrane curvatures (CB_1 and opsin, inside out). Thus, the sign of the curvature does not influence to a measurable extent the effect of membrane bending on the oligomerization of the three GPCRs that we examined.

Previously, we used the Wolber and Hudson model to determine the standard Gibbs free energy of association and the FRET efficiency within the β_2AR dimer (E_{bound}) to be ~0.2 for proteoliposomes of 120–130 nm in diameter (20). Assuming that the dimeric complexes on average interact at the same interfaces independently of curvature (i.e., E_{bound} is constant), we can now estimate the fraction of bound dimers as a function of curvature (see Supporting Materials and Methods, Estimation of β_2AR Association Energies as a Function of Membrane Curvature). Our estimate yields a curvature-imposed change in association energy from −7.8 kcal/mole in quasi-planar bilayers to −3.8 kcal/mole in highly curved membranes (Fig. 3 *C*). A ~4 kcal/mole change is significantly larger than the cost of structural TMP mutations (55), revealing the pronounced effect of membrane curvature on dimer stability.

To gain insight on the possible underlying mechanisms driving the difference in dimerization at higher membrane curvature, we developed the following theoretical framework. We evaluated the dimerization on-rate constant and its dependence on membrane curvature using protein mobility theory in combination with a diffusion-limited on-rate constant (56) (see Fig. 3 *D* and Supporting Materials and Methods, Calculation of β_2AR On-Rates). We found that the theoretical diffusion constant is much lower in highly curved membranes (1.9 $\mu m^2/s$) compared to a planar bilayer (3.9 $\mu m^2/s$). We estimated the dimerization on-rate constant under the assumption that a dimer-binding reaction will take place every time that two receptors collide (diffusion-limited dimerization). Under this assumption, a diffusion constant that increases with the vesicle diameter implies an on-rate constant that decreases in highly curved membranes (Fig. 3 *D*). Furthermore, by combining our measured association free-energy with the diffusion-limited dimerization model and estimates of the dimerization on-rate, we were able to calculate the approximate dimer lifetimes as a function of membrane curvature (Fig. 3 *E*). Notably, the combined effect of increased on-rate (faster diffusion) and increased association energy (increased stability of the dimers) predicted a significant increase (by three orders of magnitude) in the dimer lifetime of planar membranes.

Our results demonstrate that the geometry of the membrane environment strongly modulates GPCR oligomerization. Changes in local membrane environments, whether from the dynamic rearrangements of plasma membrane or via cycling to endosomes or nanotubules, are thus predicted to regulate the oligomeric lifetime of GPCRs.

Soluble ligands do not perturb the influence of membrane curvature or GPCR stoichiometry

There has been considerable effort in the GPCR oligomerization field to resolve whether ligands modify class A GPCR receptor oligomerization, with a body of studies with opposing conclusions (compare (23,57,58) to (42,59–61)). Here, we chose to evaluate the effect of ligands for the β_2AR because of its outside-out orientation in proteoliposomes, which allows ligands to bind from solution. We previously tested the influence of the β_2AR agonist (isoproterenol (ISO)) and inverse agonist ((2R,3R)-rel-3-isopropylamino-1-(7-methylindan-4-yloxy)-butan-2-ol hydrochloride (ICI) 118,551) by fitting the scaling of E_{FRET} with density (20). We observed an approximately threefold increase of K_a for ICI, suggesting that ligands have the potential to modulate the inherent propensity of β_2AR oligomerization.

Here, we first tested the influence of ligand binding on the curvature-dependent oligomerization behavior. We incubated β_2AR proteoliposomes with saturating concentrations of ISO (10 μM) and ICI (500 nM) for 30 min before imaging (see Supporting Materials and Methods, Ligands). To evaluate the effect of membrane curvature on oligomerization, we chose a constant protein density (see Fig. S3). The presence of either ligand (Fig. 4 *A*) did not perturb to a measurable extent the effect of membrane curvature on oligomerization, thus suggesting that the regulation by membrane curvature is unaffected by ligand binding.

We next tested the effect of ligands on the apparent oligomer stoichiometry, here including all receptor densities and proteoliposome diameters (Fig. 4 *B*). We found that the apparent average stoichiometry of β_2AR 1.8 ± 0.2 did

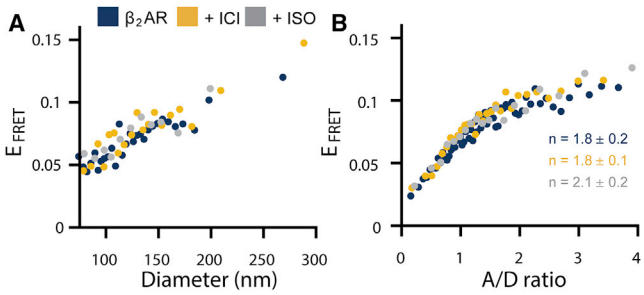

FIGURE 4 Effect of ligands on β_2AR oligomerization. (*A*) β_2AR oligomerization and (*B*) apparent average β_2AR stoichiometry are shown as a function of membrane curvature under saturating conditions of either agonist isoproterenol (ISO) or inverse agonist ICI 118,551 (ICI). Data in (*A*) have a constant receptor density and A/D ratio (Fig. S3). In (*A*), data were binned (75 proteoliposomes per bin), and a weighted average is shown. Data in (*A*) comprise a total of $n > 900$ single proteoliposomes for each ligand condition. In (*B*), data were binned (200 single proteoliposomes per bin), and a weighted average is shown. Data in (*B*) comprise a total of $n > 4000$ single proteoliposomes for each ligand condition. Uncertainties in (*A*) and (*B*) are less than or equal to the displayed marker size. Taken together, we find that ligands do not perturb the influence of membrane curvature or the stoichiometry of β_2AR.

not change in the presence of ICI, 1.8 ± 0.1, or ISO, 2.1 ± 0.2. These results are in line with single-molecule tracking studies in live cells in which ISO was shown not to influence the stoichiometry of β_2AR (42).

Although agonist (ISO) and inverse agonist (ICI) binding has been shown to induce different ligand-bound conformational states in β_2AR monomers (62,63), we found here that these ligands did not alter the strong regulatory effect of the membrane or translate into a change in average stoichiometry. Our data suggest that both the influence of membrane curvature and the conserved dimeric β_2AR stoichiometry are fundamental to different ligand-bound conformational states of the receptor.

DISCUSSION

The oligomerization of class A GPCRs has been studied extensively, and accumulating evidence support that GPCRs can, in principle, form dimeric or oligomeric assemblies in the plasma membrane (5). However, many reports arrive at conflicting conclusions regarding the existence, stability, and stoichiometry as well as the influence of endogenous and pharmacological ligands on these assemblies (6–8,33). The majority of GPCR oligomerization studies have been performed in living cells (9), in which many environmental effectors may influence oligomerization. Here, we exploited a recently developed methodology based on HCA of single proteoliposomes to provide a comprehensive analysis of GPCR oligomerization unbiased by cellular complexity and intrareconstitution proteoliposome heterogeneities. Our results demonstrate that GPCR oligomerization is receptor specific and highly sensitive to environmental effectors, such as local protein density and membrane curvature, and we propose that this could in part explain the inconsistencies present in the published literature.

We directly compared the oligomerization behavior of three GPCRs with distinct biological roles (β_2AR, CB_1, and opsin) to identify key similarities and differences in their oligomerization propensity. The three receptors associated with vastly different strengths, ranging from the relatively weak association of β_2AR to the very strong association of opsin (Fig. 2 *B*). The apparent Gibbs free energy of association for β_2AR (−3.9 ± 0.007 kcal/mole) is slightly higher than what has been reported for the dimerization of a model transmembrane helix in liposomes (−3.0 kcal/mole) (64), which was considered to be reduced to the simplest TMP interaction in lipid membranes. This free energy of association meant that in proteoliposomes, β_2AR oligomerization was predominantly modulated for surface densities between 300 and 2000 receptors/μm^2 (Fig. 2 *B*). Interestingly, β_2AR in H9C2 cardiomyocyte-like cells (65) is clustered within plasma membrane regions of ∼ 120–160 nm in diameter with very similar densities (∼600–6400 receptors/μm^2) (65). It is noteworthy that when receptors are clustered, their density is not uniform over the entire plasma membrane; thus, the average density estimated with ensemble average methods like radio ligand binding can underestimate by a factor of ∼100 or more the real local density (65).

The apparent Gibbs free energy of association for CB_1 (−15.2 ± 0.8 kcal/mole) was much lower than that of β_2AR, reflecting the propensity of CB_1 to form oligomers at much lower receptor densities than β_2AR and revealing that CB_1 is able to readily form high-energy oligomers in the absence of cellular coagents. We found that opsin had an even lower association energy than CB_1, which we could not determine because it remained almost fully oligomerized over the density range covered in our experiment (corresponding to 300–3000 receptors/μm^2). The differences that we quantified in oligomer energetics imply that the GPCR monomer-oligomer association reaction can be regulated in a receptor-specific manner. Such specificity would allow cellular effectors to fine-tune the interaction strength and oligomerization state for each receptor in different regions of the cell; thus, providing a means to locally modulate GPCR function.

Dimer dissociation constants in units of receptors/μm^2 have been reported for two other class A GPCRs in model cell studies; namely, the N-formyl peptide receptor in Chinese hamster ovary cells (59) (3.6 receptors/μm^2) and opsin in COS-7 cells (66) (1010 receptors/μm^2). These results suggest that opsin would be the weaker dimer; however, they are obtained in two different cell lines and thus may not be directly comparable. For example, a recent study revealed that β_2AR formed clusters in cardiomyocytes but not in HeLa or Chinese hamster ovary cell lines when examined systematically, side by side, by super-resolution photoactivated localization microscopy (67).

It is worth highlighting that the association strengths of interaction for oligomers of different sizes are best compared in units of kilocalories/mole or kilojoules/mole. Considering that the dimer and tetramer reaction schemes [M] + [M] ↔ [D] and [M] + [M] + [M] + [M] ↔ [T] (M denotes monomer, D denotes dimer, and T denotes tetramer), the association constants $K_{A,dimer} = [D]/[M]^2$ and $K_{A,tetramer} = [D]/[M]^4$ have different units of $[concentration]^{-1}$ and $[concentration]^{-3}$, respectively. This is also the case when converting association constants into a characteristic length scale such as concentration of receptors per area. Furthermore, converting to a characteristic length scale in the relevant dimension of the membrane solvent is not trivial (68) and would require generalizing assumptions on lipid parameters such as membrane thickness or lipid headgroup area (69), both of which are highly variable between and within cells and influential on association energetics (64). We therefore overall suggest comparing the strengths of interaction on the energy scale in our study.

The apparent average stoichiometry varied greatly among the receptors. β_2AR was dimeric, whereas opsin and CB_1

were tetrameric and pentameric, respectively (Fig. 2 *A*), suggesting that CB_1 and opsin have multiple interfaces of interaction to accommodate higher-order oligomers. Accumulating evidence from single-molecule studies in live cells suggests that class A GPCR oligomers form reversibly (42,59,70,71) and comprise mixtures of monomers, dimers, and higher-order oligomers (42,71). We could test the existence of mixed oligomeric species in our samples by monitoring changes in the apparent average stoichiometry as a function of total receptor concentration. The average stoichiometry of CB_1 increased with density (Fig. 2 *C*) as expected, suggesting a shift from predominately dimeric to predominantly pentameric clusters. Surprisingly, we did not observe the same behavior for β_2AR, which exhibited a constant (dimeric) average apparent stoichiometry over the entire density range investigated ($\sim$300–3000 receptors/μm^2). This is in contrast with a live cell single-particle tracking study of β_2AR (42) and suggests that if β_2AR forms higher-order oligomers, then additional cellular cofactors may be required. Our findings support that GPCRs can have a preferred average stoichiometry and that the robustness of these stoichiometries to small changes in receptor density is receptor specific.

We further provide, to our knowledge, the first experimental evidence that the geometrical environment of the membrane modulates GPCRs association. Membrane curvature is rapidly regulated in living cells during signaling (e.g., in endocytosis) and is considered crucial in tuning protein recruitment to active signaling sites (72–75). Interestingly, in addition to their canonical signaling platform in the plasma membrane, GPCRs have recently been observed to function in areas of high membrane curvature such as endosomes ($<$60–500 nm) (50,76,77) and lipid nanotubules ($20 - 450$ nm) (78,79) with diameters comparable to proteoliposomes ($40 - 400$ nm, Fig. 1 *D*). We found that high membrane curvature decreased the interactions of β_2AR, CB_1, and opsin (Fig. 3 *A*; Fig. S3, *B* and *C*) and decreased their average stoichiometry (Fig. 3 *B*). We calculate that membrane curvature perturbs β_2AR association energy by $\sim$4 kcal/mole. A reduction of 4 kcal/mole in association energy is significantly larger (on average $>$1 kcal/mole higher) than the cost of systematically perturbing TMP helix-helix interactions by structural mutations (55) or the effects of ligands (20), suggesting that modulation by membrane curvature can affect also other TMP assemblies. Furthermore, coupled to the modulation in receptor mobility in curved membranes, the stability change implies order-of-magnitude variations in dimeric lifetimes, which could have profound functional consequences. Our results predict that the geometry of the local membrane environment in living cells, as observed for example in clathrin-coated pits, modulates GPCR oligomerization.

The lipid environment of the membrane likely plays a role in GPCR association in the cell (80). Here, we chose minimal lipid compositions shown to stabilize each GPCR in proteoliposomes to directly compare their oligomerization. The lipid requirements to maintain a functional β_2AR were, however, different for CB_1 and opsin (Materials and Methods). Nevertheless, we found that the response of receptors to membrane curvature remains intact for all receptors (e.g., oligomerization and stoichiometry decreased for all GPCRs in proteoliposomes with high membrane curvature (see Figs. S3, *A–C* and S4). Additionally, we found that lipid composition did not overwrite the uniqueness of receptor-receptor interactions for each GPCR, e.g., CB_1 and opsin were reconstituted under identical lipid compositions but showed distinct differences in association energies and oligomer stoichiometry as a function of density (Fig. 2, *B* and *C*).

Studies of oligomerization in a cellular context undoubtedly enhance the biological relevance of the investigation. However, our findings highlight overall that a quantitative systematic comparison between different receptors is greatly facilitated by experimental conditions that can begin to disentangle cellular complexities and nanoscale heterogeneities to reveal the intrinsic physical propensity of monomers to oligomerize. The assays introduced here are thus expected to assist the quantitative experimental observation of oligomerization for TMPs in general.

SUPPORTING MATERIAL

Supporting Materials and Methods, four figures, and one table are available at http://www.biophysj.org/biophysj/supplemental/S0006-3495(18)30677-5.

AUTHOR CONTRIBUTIONS

D.S. conceived of the strategy and was responsible for overall project management and supervision. S.M.W., S.M., S.M.C., and D.S. designed all the experiments. S.G.F.R. and J.J.F. expressed, purified, labeled, and reconstituted the β_2AR. J.F.F. expressed, purified, labeled, and reconstituted the CB_1 and opsin. S.M.W. and S.M. performed the fluorescence measurements, data analysis, and theoretical calculations. C.K. and K.H. determined the association energies. D.P and E.B. performed the theoretical calculations for curvature effects on receptor diffusion and dimer lifetime. S.M.W., S.M., S.M.C., and D.S. wrote the article. All authors discussed the results and commented on the article.

ACKNOWLEDEMENTS

This work was supported by the Danish Council for Strategic Research (grant number 1311-00002B) and Innovation Fund Denmark (grant number 5184-00048B). Partial funds were provided by National Institutes of Health grants DA038882 and DA026434 (to M.F.). E.B. was supported in part by National Institute on Drug Abuse grant T32 DA007135.

SUPPORTING CITATIONS

References (81–89) appear in the Supporting Material.

REFERENCES

1. Rosenbaum, D. M., S. G. Rasmussen, and B. K. Kobilka. 2009. The structure and function of G-protein-coupled receptors. *Nature.* 459:356–363.
2. Audet, M., and M. Bouvier. 2012. Restructuring G-protein- coupled receptor activation. *Cell.* 151:14–23.
3. Ferré, S., V. Casadó, …, X. Guitart. 2014. G protein-coupled receptor oligomerization revisited: functional and pharmacological perspectives. *Pharmacol. Rev.* 66:413–434.
4. Levitz, J., C. Habrian, …, E. Y. Isacoff. 2016. Mechanism of assembly and cooperativity of homomeric and heteromeric metabotropic glutamate receptors. *Neuron.* 92:143–159.
5. Milligan, G. 2013. The prevalence, maintenance, and relevance of G protein-coupled receptor oligomerization. *Mol. Pharmacol.* 84:158–169.
6. Vischer, H. F., M. Castro, and J. P. Pin. 2015. G protein-coupled receptor multimers: a question still open despite the use of novel approaches. *Mol. Pharmacol.* 88:561–571.
7. Lambert, N. A., and J. A. Javitch. 2014. CrossTalk opposing view: weighing the evidence for class A GPCR dimers, the jury is still out. *J. Physiol.* 592:2443–2445.
8. Bouvier, M., and T. E. Hébert. 2014. CrossTalk proposal: weighing the evidence for class A GPCR dimers, the evidence favours dimers. *J. Physiol.* 592:2439–2441.
9. Kasai, R. S., and A. Kusumi. 2014. Single-molecule imaging revealed dynamic GPCR dimerization. *Curr. Opin. Cell Biol.* 27:78–86.
10. Chung, I., R. Akita, …, I. Mellman. 2010. Spatial control of EGF receptor activation by reversible dimerization on living cells. *Nature.* 464:783–787.
11. Head, B. P., H. H. Patel, and P. A. Insel. 2014. Interaction of membrane/lipid rafts with the cytoskeleton: impact on signaling and function: membrane/lipid rafts, mediators of cytoskeletal arrangement and cell signaling. *Biochim. Biophys. Acta.* 1838:532–545.
12. Berridge, M. J. 2014. Module 2: cell signalling pathways. *Cell Signal. Biol* Published online October 1, 2014. https://doi.org/10.1042/csb0001022.
13. Baumgart, F., and G. J. Schütz. 2015. Detecting protein association at the T cell plasma membrane. *Biochim. Biophys. Acta.* 1853:791–801.
14. Mansoor, S. E., K. Palczewski, and D. L. Farrens. 2006. Rhodopsin self-associates in asolectin liposomes. *Proc. Natl. Acad. Sci. USA.* 103:3060–3065.
15. Rigaud, J. L., and D. Lévy. 2003. Reconstitution of membrane proteins into liposomes. *Methods Enzymol.* 372:65–86.
16. Niu, S. L., B. Doctrow, and D. C. Mitchell. 2009. Rhodopsin activity varies in proteoliposomes prepared by different techniques. *Biochemistry.* 48:156–163.
17. Larsen, J., N. S. Hatzakis, and D. Stamou. 2011. Observation of inhomogeneity in the lipid composition of individual nanoscale liposomes. *J. Am. Chem. Soc.* 133:10685–10687.
18. Chen, X., D. Araç, …, J. Rizo. 2006. SNARE-mediated lipid mixing depends on the physical state of the vesicles. *Biophys. J.* 90:2062–2074.
19. Kimura, T., A. A. Yeliseev, …, K. Gawrisch. 2012. Recombinant cannabinoid type 2 receptor in liposome model activates g protein in response to anionic lipid constituents. *J. Biol. Chem.* 287:4076–4087.
20. Mathiasen, S., S. M. Christensen, …, D. Stamou. 2014. Nanoscale high-content analysis using compositional heterogeneities of single proteoliposomes. *Nat. Methods.* 11:931–934.
21. Howlett, A. C., L. C. Blume, and G. D. Dalton. 2010. CB(1) cannabinoid receptors and their associated proteins. *Curr. Med. Chem.* 17:1382–1393.
22. Palczewski, K. 2006. G protein-coupled receptor rhodopsin. *Annu. Rev. Biochem.* 75:743–767.
23. Fung, J. J., X. Deupi, …, B. K. Kobilka. 2009. Ligand-regulated oligomerization of β(2)-adrenoceptors in a model lipid bilayer. *EMBO J.* 28:3315–3328.
24. Fay, J. F., and D. L. Farrens. 2017. Purification of functional CB1 and analysis by site-directed fluorescence labeling methods. *Methods Enzymol.* 593:343–370.
25. Xie, G., A. K. Gross, and D. D. Oprian. 2003. An opsin mutant with increased thermal stability. *Biochemistry.* 42:1995–2001.
26. Fay, J. F., and D. L. Farrens. 2012. A key agonist-induced conformational change in the cannabinoid receptor CB1 is blocked by the allosteric ligand Org 27569. *J. Biol. Chem.* 287:33873–33882.
27. Ridge, K. D., Z. Lu, …, H. G. Khorana. 1995. Structure and function in rhodopsin. Separation and characterization of the correctly folded and misfolded opsins produced on expression of an opsin mutant gene containing only the native intradiscal cysteine codons. *Biochemistry.* 34:3261–3267.
28. Tsukamoto, H., A. Sinha, …, D. L. Farrens. 2010. Monomeric rhodopsin is the minimal functional unit required for arrestin binding. *J. Mol. Biol.* 399:501–511.
29. Periasamy, A., H. Wallrabe, …, M. Barroso. 2008. Chapter 22: quantitation of protein-protein interactions: confocal FRET microscopy. *Methods Cell Biol.* 89:569–598.
30. McCann, J. J., U. B. Choi, …, M. E. Bowen. 2010. Optimizing methods to recover absolute FRET efficiency from immobilized single molecules. *Biophys. J.* 99:961–970.
31. Bendix, P. M., M. S. Pedersen, and D. Stamou. 2009. Quantification of nano-scale intermembrane contact areas by using fluorescence resonance energy transfer. *Proc. Natl. Acad. Sci. USA.* 106:12341–12346.
32. Stamou, D., C. Duschl, …, H. Vogel. 2003. Self-assembled microarrays of attoliter molecular vessels. *Angew. Chem. Int.Engl.* 42:5580–5583.
33. Lan, T. H., Q. Liu, …, N. A. Lambert. 2015. BRET evidence that β2 adrenergic receptors do not oligomerize in cells. *Sci. Rep.* 5:10166.
34. Mercier, J. F., A. Salahpour, …, M. Bouvier. 2002. Quantitative assessment of β 1- and β 2-adrenergic receptor homo- and heterodimerization by bioluminescence resonance energy transfer. *J. Biol. Chem.* 277:44925–44931.
35. Meyer, B. H., J. M. Segura, …, H. Vogel. 2006. FRET imaging reveals that functional neurokinin-1 receptors are monomeric and reside in membrane microdomains of live cells. *Proc. Natl. Acad. Sci. USA.* 103:2138–2143.
36. James, J. R., M. I. Oliveira, …, S. J. Davis. 2006. A rigorous experimental framework for detecting protein oligomerization using bioluminescence resonance energy transfer. *Nat. Methods.* 3:1001–1006.
37. Adair, B. D., and D. M. Engelman. 1994. Glycophorin A helical transmembrane domains dimerize in phospholipid bilayers: a resonance energy transfer study. *Biochemistry.* 33:5539–5544.
38. Veatch, W., and L. Stryer. 1977. The dimeric nature of the gramicidin A transmembrane channel: conductance and fluorescence energy transfer studies of hybrid channels. *J. Mol. Biol.* 113:89–102.
39. Clegg, R. M. 1995. Fluorescence resonance energy transfer. *Curr. Opin. Biotechnol.* 6:103–110.
40. King, C., V. Raicu, and K. Hristova. 2017. Understanding the FRET signatures of interacting membrane proteins. *J. Biol. Chem.* 292:5291–5310.
41. Angers, S., A. Salahpour, …, M. Bouvier. 2000. Detection of β 2-adrenergic receptor dimerization in living cells using bioluminescence resonance energy transfer (BRET). *Proc. Natl. Acad. Sci. USA.* 97:3684–3689.
42. Calebiro, D., F. Rieken, …, M. J. Lohse. 2013. Single-molecule analysis of fluorescently labeled G-protein-coupled receptors reveals complexes with distinct dynamics and organization. *Proc. Natl. Acad. Sci. USA.* 110:743–748.

43. Fotiadis, D., Y. Liang, …, K. Palczewski. 2003. Atomic-force microscopy: rhodopsin dimers in native disc membranes. *Nature.* 421:127–128.

44. Jastrzebska, B., D. Fotiadis, …, K. Palczewski. 2006. Functional and structural characterization of rhodopsin oligomers. *J. Biol. Chem.* 281:11917–11922.

45. Gunkel, M., J. Schöneberg, …, A. Al-Amoudi. 2015. Higher-order architecture of rhodopsin in intact photoreceptors and its implication for phototransduction kinetics. *Structure.* 23:628–638.

46. Wolber, P. K., and B. S. Hudson. 1979. An analytic solution to the Förster energy transfer problem in two dimensions. *Biophys. J.* 28:197–210.

47. Raicu, V. 2007. Efficiency of resonance energy transfer in homo-oligomeric complexes of proteins. *J. Biol. Phys.* 33:109–127.

48. Patowary, S., L. F. Pisterzi, …, V. Raicu. 2015. Experimental verification of the kinetic theory of FRET using optical microspectroscopy and obligate oligomers. *Biophys. J.* 108:1613–1622.

49. Domanov, Y. A., S. Aimon, …, P. Bassereau. 2011. Mobility in geometrically confined membranes. *Proc. Natl. Acad. Sci. USA.* 108:12605–12610.

50. Irannejad, R., J. C. Tomshine, …, M. von Zastrow. 2013. Conformational biosensors reveal GPCR signalling from endosomes. *Nature.* 495:534–538.

51. Tonnesen, A., S. M. Christensen, …, D. Stamou. 2014. Geometrical membrane curvature as an allosteric regulator of membrane protein structure and function. *Biophys. J.* 106:201–209.

52. Callan-Jones, A., B. Sorre, and P. Bassereau. 2011. Curvature-driven lipid sorting in biomembranes. *Cold Spring Harb. Perspect. Biol.* 3:a004648.

53. Rosholm, K. R., N. Leijnse, …, D. Stamou. 2017. Membrane curvature regulates ligand-specific membrane sorting of GPCRs in living cells. *Nat. Chem. Biol.* 13:724–729.

54. Prévost, C., H. Zhao, …, P. Bassereau. 2015. IRSp53 senses negative membrane curvature and phase separates along membrane tubules. *Nat. Commun.* 6:8529.

55. Doura, A. K., and K. G. Fleming. 2004. Complex interactions at the helix-helix interface stabilize the glycophorin A transmembrane dimer. *J. Mol. Biol.* 343:1487–1497.

56. Torney, D. C., and H. M. McConnell. 1983. Diffusion-limited reaction rate theory for two-dimensional systems. *Proc. Math. Phys. Eng. Sci.* 387:147–170.

57. Alvarez-Curto, E., R. J. Ward, …, G. Milligan. 2010. Ligand regulation of the quaternary organization of cell surface M3 muscarinic acetylcholine receptors analyzed by fluorescence resonance energy transfer (FRET) imaging and homogeneous time-resolved FRET. *J. Biol. Chem.* 285:23318–23330.

58. Ganguly, S., A. H. Clayton, and A. Chattopadhyay. 2011. Organization of higher-order oligomers of the serotonin$_1$(A) receptor explored utilizing homo-FRET in live cells. *Biophys. J.* 100:361–368.

59. Kasai, R. S., K. G. Suzuki, …, A. Kusumi. 2011. Full characterization of GPCR monomer-dimer dynamic equilibrium by single molecule imaging. *J. Cell Biol.* 192:463–480.

60. Herrick-Davis, K., E. Grinde, …, J. E. Mazurkiewicz. 2012. Oligomer size of the serotonin 5-hydroxytryptamine 2C (5-HT2C) receptor revealed by fluorescence correlation spectroscopy with photon counting histogram analysis: evidence for homodimers without monomers or tetramers. *J. Biol. Chem.* 287:23604–23614.

61. Goin, J. C., and N. M. Nathanson. 2006. Quantitative analysis of muscarinic acetylcholine receptor homo- and heterodimerization in live cells: regulation of receptor down-regulation by heterodimerization. *J. Biol. Chem.* 281:5416–5425.

62. Rasmussen, S. G., H. J. Choi, …, B. K. Kobilka. 2011. Structure of a nanobody-stabilized active state of the β(2) adrenoceptor. *Nature.* 469:175–180.

63. Manglik, A., T. H. Kim, …, B. K. Kobilka. 2015. Structural insights into the dynamic process of β2-adrenergic receptor signaling. *Cell.* 161:1101–1111.

64. Yano, Y., and K. Matsuzaki. 2006. Measurement of thermodynamic parameters for hydrophobic mismatch 1: self-association of a transmembrane helix. *Biochemistry.* 45:3370–3378.

65. Ianoul, A., D. D. Grant, …, J. P. Pezacki. 2005. Imaging nanometer domains of β-adrenergic receptor complexes on the surface of cardiac myocytes. *Nat. Chem. Biol.* 1:196–202.

66. Comar, W. D., S. M. Schubert, …, A. W. Smith. 2014. Time-resolved fluorescence spectroscopy measures clustering and mobility of a G protein-coupled receptor opsin in live cell membranes. *J. Am. Chem. Soc.* 136:8342–8349.

67. Scarselli, M., P. Annibale, and A. Radenovic. 2012. Cell type-specific β2-adrenergic receptor clusters identified using photoactivated localization microscopy are not lipid raft related, but depend on actin cytoskeleton integrity. *J. Biol. Chem.* 287:16768–16780.

68. Fleming, K. G. 2002. Standardizing the free energy change of transmembrane helix-helix interactions. *J. Mol. Biol.* 323:563–571.

69. Provasi, D., J. M. Johnston, and M. Filizola. 2010. Lessons from free energy simulations of δ-opioid receptor homodimers involving the fourth transmembrane helix. *Biochemistry.* 49:6771–6776.

70. Hern, J. A., A. H. Baig, …, N. J. Birdsall. 2010. Formation and dissociation of M1 muscarinic receptor dimers seen by total internal reflection fluorescence imaging of single molecules. *Proc. Natl. Acad. Sci. USA.* 107:2693–2698.

71. Cai, X., B. Bai, …, J. Chen. 2017. Apelin receptor homodimer-oligomers revealed by single-molecule imaging and novel G protein-dependent signaling. *Sci. Rep.* 7:40335.

72. Henne, W. M., E. Boucrot, …, H. T. McMahon. 2010. FCHo proteins are nucleators of clathrin-mediated endocytosis. *Science.* 328:1281–1284.

73. Antonny, B. 2011. Mechanisms of membrane curvature sensing. *Annu. Rev. Biochem.* 80:101–123.

74. Hatzakis, N. S., V. K. Bhatia, …, D. Stamou. 2009. How curved membranes recruit amphipathic helices and protein anchoring motifs. *Nat. Chem. Biol.* 5:835–841.

75. Aimon, S., A. Callan-Jones, …, P. Bassereau. 2014. Membrane shape modulates transmembrane protein distribution. *Dev. Cell.* 28:212–218.

76. McMahon, H. T., and E. Boucrot. 2011. Molecular mechanism and physiological functions of clathrin-mediated endocytosis. *Nat. Rev. Mol. Cell Biol.* 12:517–533.

77. Krauss, M., and V. Haucke. 2009. Shaping membranes for endocytosis. *Rev. Physiol. Biochem. Pharmacol.* 161:45–66.

78. Nikolaev, V. O., A. Moshkov, …, J. Gorelik. 2010. β2-adrenergic receptor redistribution in heart failure changes cAMP compartmentation. *Science.* 327:1653–1657.

79. Ibrahim, M., J. Gorelik, …, C. M. Terracciano. 2011. The structure and function of cardiac t-tubules in health and disease. *Proc. Biol. Sci.* 278:2714–2723.

80. Soubias, O., and K. Gawrisch. 2012. The role of the lipid matrix for structure and function of the GPCR rhodopsin. *Biochim. Biophys. Acta.* 1818:234–240.

81. Fay, J. F., T. D. Dunham, and D. L. Farrens. 2005. Cysteine residues in the human cannabinoid receptor: only C257 and C264 are required for a functional receptor, and steric bulk at C386 impairs antagonist SR141716A binding. *Biochemistry.* 44:8757–8769.

82. Kunding, A. H., M. W. Mortensen, …, D. Stamou. 2008. A fluorescence-based technique to construct size distributions from single-object measurements: application to the extrusion of lipid vesicles. *Biophys. J.* 95:1176–1188.

83. Ulbrich, M. H., and E. Y. Isacoff. 2007. Subunit counting in membrane-bound proteins. *Nat. Methods.* 4:319–321.

84. Press, W. H., B. P. Flannery, …, W. T. Vetterling. 1989. Numerical Recipes in C: The Art of Scientific Computing. Cambridge University Press, Cambridge, UK.

85. King, C., S. Sarabipour, …, K. Hristova. 2014. The FRET signatures of noninteracting proteins in membranes: simulations and experiments. *Biophys. J.* 106:1309–1317.

86. Kenworthy, A. K., and M. Edidin. 1998. Distribution of a glycosylphosphatidylinositol-anchored protein at the apical surface of MDCK cells examined at a resolution of <100 A using imaging fluorescence resonance energy transfer. *J. Cell Biol.* 142:69–84.

87. Marrink, S. J., A. H. De Vries, and A. E. Mark. 2004. Coarse grained model for semiquantitative lipid simulations. *J. Phys. Chem. B.* 108:750–760.

88. Saffman, P. G., and M. Delbrück. 1975. Brownian motion in biological membranes. *Proc. Natl. Acad. Sci. USA.* 72:3111–3113.

89. Henle, M. L., and A. J. Levine. 2010. Hydrodynamics in curved membranes: the effect of geometry on particulate mobility. *Phys. Rev. E Stat. Nonlin. Soft Matter Phys.* 81:011905.

Biophysical Journal, Volume *115*

Supplemental Information

Single Proteoliposome High-Content Analysis Reveals Differences in the Homo-Oligomerization of GPCRs

Samuel M. Walsh, Signe Mathiasen, Sune M. Christensen, Jonathan F. Fay, Christopher King, Davide Provasi, Ernesto Borrero, Søren G.F. Rasmussen, Juan Jose Fung, Marta Filizola, Kalina Hristova, Brian Kobilka, David L. Farrens, and Dimitrios Stamou

Single proteoliposome high content analysis reveals differences in the homo-oligomerization of GPCRs

Supporting Material

S. M. Walsh, S. Mathiasen, S. M. Christensen, J. F. Fay, C. King, D. Provasi, E. Borrero, S. G. F. Rasmussen, J. J. Fung, M. Filizola, K. Hristova, B. Kobilka, D. L. Farrens, D. Stamou

Contents

1 SUPPORTING MATERIALS AND METHODS

1.1 Engineered receptor constructs

Receptor constructs were engineered with a specific cysteine labeling site for fluorescent labeling on the surface exposed part of Helix 8 (H8).

B_2AR labelled at H8 position R333C (1): This construct was termed Δ5. Five cysteines were mutated and substituted respectively with (C77V, C265A, C327S, C378A and C406A). Subsequently, a single cysteine was introduced at R333C for specific labelling.

CB_1 labelled at H8 position A407C (2): Minimal cysteine truncated purification construct (Δ88/Δ417) termed θ, in which only two of the 13 endogenous cysteines (Cys-257 and Cys-264) were retained to ensure a functional receptor (2). A specific cysteine for labelling was introduced at A407C.

Opsin labelled at Helix 8 position 316C (3, 4): The construct termed θ' was created using a well characterized non-reactive labelling construct (140S, 167S, 222S, 264S, 322S, and 323S) (4). Into this construct two cysteines were introduced (N2C, D282C) to thermally stabilize the apo protein opsin (3). The endogenous 316C was used for specific labelling.

1.2 Orientation of receptors

The orientation of β_2AR was previously determined by Fung et al. (1) to be ~90% outside out. The orientation of CB_1 and opsin was determined by digestion of the receptors C-terminal region with V8 protease and the concurrent loss of the rhodopsin 1D4 epitope (TETSQVAPA) (5). The 1D4 epitope was used to aid in receptor purification (see (5)). Immunoblot analysis with the 1D4 monoclonal antibody in **Fig. S1** shows that CB_1 and opsin are orientated with the extracellular domain inside the proteoliposome (inside out).

1.3 Determining fluorescent signal correction factors (ω, α, β)

To accurately determine $E_{FRET,}$ fluorescent signals were carefully corrected for fluorescence contaminations using correction factors (ω, α, β) (see **Quantification of E_{FRET} (Materials and Methods)**). We used three control samples (preparations 2-4 described in **Proteoliposome preparation (Materials and Methods))** and imaged these employing the exact same microscopy conditions as for the proteoliposomes investigated for FRET (preparation 1). Correction factors were determined separately for β_2AR and for CB_1 and opsin samples to account for smaller changes in the microscope alignments and to accommodate a potential requirement for re-optimization of laser and image settings. All correction factors are reported as mean ± sem determined from hundreds (n) of single proteoliposomes. In the following section superscript ^{0} denotes raw uncorrected intensities. I_D and $I_A^{0,FRET}$ are the donor and acceptor intensity excited by the donor laser line (543 nm).

ω was determined using the control sample labeled only by OG-DHPE (preparation 2) and represents the ratio of OG intensity in the I_D^0 channel to OG intensity in the membrane channel (I_M^0) when excited with the 476 nm laser. ω was determined to be 0.9 ± 0.02% for β_2AR (n = 729) (13) and (3.3 ± 0.0004%) (n = 1163) for CB_1 and opsin.

β was determined using the control sample harboring only GPCR-Cy3 (preparation 3) and represents the ratio of Cy3 intensity in the acceptor emission channel to Cy3 intensity in the donor emission channel when excited with the 543 nm laser. β was determined to be (11.1 ± 0.06%) for β_2AR (n = 1130) (13), (14.5 ± 0.001%) for CB_1 (n = 1399) and (13.3 ± 0.001%) for opsin (n = 1630).

α was determined using the control sample harboring GPCR-Cy5 only (preparation 4) and represents the ratio of Cy5 intensity in the acceptor channel when excited by the 543 nm laser to the intensity of Cy5 intensity in the acceptor channel excited by the 633 nm laser. α was determined to be (9.8 ± 0.1%) for β_2AR (n = 1130) (13), (6.7 ± 0.001%) for CB_1 (n = 1399) and (6.2 ± 0.001%) for opsin (n = 1630).

1.4 Proteoliposome size

Proteoliposome diameters were determined as described previously (6, 9, 10) by relating the fluorescence intensity of the proteoliposome membrane fluorophore OG-DHPE to proteoliposome diameter as measured by dynamic light scattering (DLS). Briefly, because the number of fluorophores incorporated in the membrane (Oregon Green-DHPE) is proportional to the proteoliposome surface area and thereby related to diameter (D) through Eq. S1, a conversion from diffraction limited intensity spots to physical proteoliposome size was possible.

$$I_{Oregon\ Green\ DHPE} \propto A_{Liposome} = \pi D_{Liposome}^2$$
$$\Rightarrow D_{Liposome} = C_{cal}\sqrt{I_{Oregon\ Green\ DHPE}} \qquad [S1]$$

The calibration factor (C_{cal}) was determined by the use of a calibration sample, where empty liposomes were extruded 20× through two 50 nm filters (Millipore) to produce a narrow size distribution. The calibration sample was first examined by DLS to obtain a mean diameter, and then by confocal microscopy utilizing identical imaging conditions as for GPCR-Cy3 and GPCR-Cy5 (preparation 1). The mean of the integrated Oregon Green-DHPE intensity spots was correlated to the mean radius found by DLS to obtain C_{cal}. When C_{cal} was determined all intensities were converted to diameters by Eq. S1. DLS measurements were performed on an ALV-5000 correlator equipped with a 633 nm laser. The concentration of liposomes was 0.1 g/l, and all data were collected at room temperature.

1.5 Receptor density

To calibrate receptor densities we used the fluorescent intensities from either control samples harboring only GPCR-Cy3 (preparation 3) and only GPCR-Cy5 (preparation 4) and the calculated single proteoliposome surface area. The integrated intensity of the labeled receptor $I_{A/D}$ is proportional to the number of fluorophores, and thus the number of proteins, since each receptor carries one label. This holds true for acceptor fluorophores excited by acceptor laserline (633 nm) however donor intensities are quenched by FRET. To recover the unquenched donor intensity we added the corrected acceptor FRET intensity to I_D (7), using an I_A^{FRET} that was decoupled from instrumental and photo-physical effects through the γ-factor.

We collected single molecule bleaching traces for control samples preparation 3 and preparation 4. Bleaching movies were acquired on a Leica DMI6000 TIRF setup using an oil

immersion objective HCX PL APO CS (100× magnification, 1.46 NA) (Leica). Oregon Green-DHPE, GPCR-Cy3 and GPCR-Cy5 were excited by a 488 nm laserline, a 561 nm laserline and a 635 nm laserline respectively. Oregon Green emission was filtered through a filtercube with a dichroic mirror Q495LP and a bandpass filter HQ525/50m. Cy3 emission was filtered through a filtercube with a dichroic mirror T565LP and a bandpass filter ET605/70m. Cy5 emission was filtered through a filtercube with a dichroic mirror Q660LP and a bandpass filter HQ700/75m. All filters and dichroic mirrors were from Chroma Technology. The fluorescence intensity was collected on an electron-multiplying Andor Ixon 897 camera. Images were acquired in the format of 512×512 pixels, each pixel corresponding to 160 nm sample length, bit-depth of 14 and 250 ms exposure time. Each frame was transferred in 0.304 s, bleaching series were acquired for 900 frames. Single molecule bleaching trace intensities were extracted by software written in Igor Pro Ver. 6.01 (Wavemetrics). Single molecule bleaching step intensities were quantified by subtracting the average step intensity by the average background intensity (6). For a narrow size distribution ranging from $0-60$ nm the mean number of receptor, were assessed by dividing the unbleached starting intensity by the mean bleaching step intensity (11). The mean number of receptors was correlated to the mean intensity obtained by confocal microscopy for the same narrow size range ($0-60$ nm) and this factor was used to access the number of receptors on all individual proteoliposomes.

1.6 Ensemble proteoliposome E_{FRET}

To determine the ensemble average E_{FRET} we composed a pseudo FRET efficiency by summing up all intensity signals from the imaged proteoliposome samples including signals from protein aggregates and proteoliposomes carrying only donor or acceptor labeled receptors using Eq. S2.

$$E_{bulk}^{FRET} = \frac{\frac{1}{N}\sum_N I_A^{FRET} - \beta\frac{1}{N}\sum_N I_D - \alpha\frac{1}{N}\sum_N I_A}{\frac{1}{N}\sum_N I_A^{FRET} - \beta\frac{1}{N}\sum_N I_D - \alpha\frac{1}{N}\sum_N I_A + \frac{1}{N}\sum_N I_D} \quad [S2]$$

1.7 Error propagation

The uncertainty associated with quantifying proteoliposome diameter, receptor densities, A/D ratios, and E_{FRET} were determined as described previously (6). Briefly, we propagated the errors on the 2D Gaussian fit coefficients used to determine the fluorescence intensity of each single

particle (see **Single fluorescent particle characterization (Materials and Methods)**). In **Fig. 1** ***D-G*** the full width of the propagated error histograms for the GPCR with the largest errors are shown.

1.8 Average monomer distance

We assumed receptors to be monomeric and equally distributed in the proteoliposomes. We determined the average distance between any two receptors in 3D for proteoliposomes with the highest and lowest densities. The smallest proteoliposome (40 nm diameter) with the highest density (3.0×10^{-3} receptors/nm^2) gave an average distance between any two receptors of 17 nm. Likewise, the largest proteoliposome (400 nm diameter) with the lowest observed density (0.3×10^{-3} receptors/nm^2) gave an average distance between two receptors of 58 nm.

1.9 Total receptor per assay

To estimate the total amount of receptor needed for a miniaturized screen, we used the fact that a microscope experiment required 1.5 × 106 liposomes given a microscope chamber of 5 mm in diameter and a surface density of 7.5 × 1010 proteoliposomes/m^2. Assuming each liposome carries 50 receptors of 47,058.1 g/mol each, this corresponds to 5.9 pg of protein.

1.10 Ligands

Proteoliposomes containing reconstituted β_2AR were incubated with saturating amounts (10 μM) of agonist Isoproterenol (ISO) (Sigma), and saturating amounts (500 nM) of inverse agonist ICI 118,551 (Sigma). Samples were incubated with ligands for 30 min at room temperature before measurements were taken.

1.11 Receptor stoichiometry

Using the oligomer stoichiometry theory proposed by Veatch and Stryer (12), in a modified version (13), we relate E_{FRET} to the A/D ratio and extract the apparent average oligomer stoichiometry as a fitting parameter. Here stoichiometry (n) is related to energy transfer (E_{FRET})

and maximum FRET efficiency $E_{FRETmax}$, and the mole fraction of the acceptor is represented as the acceptor to donor mole ratio (A/D ratio):

$$E_{FRET} = (1 - \frac{1}{(1+(\text{A/D ratio}))^{n-1}}) * E_{FRETmax} \quad \text{[S3]}$$

Data were fit using the Curve Fitting Toolbox in MATLAB v. 8.2 (MathWorks Inc.) evaluating *n* and $E_{FRETmax}$ as free fitting parameters. The fit was weighted with the propagated A/D ratio errors (described in **Error Propagation**).

The apparent average stoichiometry as a function of density (**Fig. 2** ***C***) only included proteoliposomes within ± 15 nm of the mean proteoliposome diameter (see **Table S1**) to avoid convoluting the effect of density with membrane curvature. The apparent average stoichiometry as a function of membrane curvature (**Fig. 3** ***B*** and **Fig. S3**) only included proteoliposomes within ± 0.2 × 10^{-3} receptors/nm^2 of the mean receptor density to avoid convoluting the effect of membrane curvature with total receptor density.

1.12 Receptor association energies

The FRET efficiencies of donor-labeled and acceptor-labeled protein oligomers were calculated using the "kinetic theory of FRET", as derived by Raicu (14, 15):

$$E_{oligo}^{Dq} = \frac{\mu_{oligo}}{[D]_T} \sum_{k=1}^{n-1} \frac{k(n-k)\tilde{E}}{1+(n-k-1)\tilde{E}} \binom{n}{k} P_D^k P_A^{n-k} \quad \text{[S4]}$$

In Eq. S4, n represents the oligomer order. μ_{oligo} is the concentration of oligomers. P_D and P_A are the fractions of donors and acceptors in the oligomer. For large numbers of molecules, P_D and P_A are equal to the fraction of donor and acceptors, respectively: x_D and x_A. $x_A = \frac{[A]}{[D]+[A]}$, with [D] and [A] representing the donor and acceptor concentrations, and $x_D + x_A = 1$. Only proteoliposomes having diameters between 120 − 130 nm were selected to avoid convoluting geometric curvature with oligomeric fraction.

Eq. S4 gives the theoretical apparent donor-quenched energy transfer efficiency for mixtures of monomers and oligomers, assuming an equal donor to acceptor distance for all D-A pairs in the oligomer. For the case of n = 2, a dimer, this is always correct as there is only one donor and one acceptor in the dimer pair. For trimers and above, this is an approximation which minimizes the number of adjustable parameters in the theoretical model for FRET (16). We fit Eq. S4 for n = 2 (β_2AR) and n = 4 (CB_1 and opsin), corresponding to the cases of monomer-dimer and monomer-

tetramer thermodynamic equilibria, to the experimental data as described below. Because CB_1 was found to form a mixture of oligomers from 2.8 ± 0.6 to 5.3 ± 0.6 in proteoliposomes with diameters between 120 – 130 nm (**Fig. 2 *C***), we chose to fit CB_1 using the average stoichiometry in this proteoliposome diameter range corresponding to a monomer-tetramer model. We determined the minimized chi-squared value for all oligomeric models. The kinetic model for FRET, however, does not take into account stochastic FRET, or FRET that occurs due to random approach of donors and acceptors in the membrane within distances of ~100 Å (14, 17). Stochastic FRET can represent a significant contribution to measured E_{FRET} in the case of a monomer-dimer equilibrium, but it decreases significantly as a function of oligomer size. As such, here we corrected for stochastic FRET in the dimer case (see (18) for details), but we did not apply a proximity FRET correction for higher order oligomers. FRET for a mixed population of monomers and dimers can be modeled as a function of the dimeric fraction $f_d(K_A,[T])$ according to Eq. S5:

$$E_{dimer}^{Dq} = f_D(K_A,[T])\, x_A \tilde{E} \quad [S5]$$

To this FRET prediction, we added a contribution for stochastic FRET (18) and completed the theoretical model for the apparent FRET efficiency for the case of a monomer-dimer equilibrium (17, 18):

$$E_{app,theory,i} = E(K_A,[A]_i)_{proximity} + x_{A,i} f_D(K,[T]_i)\tilde{E} \quad [S6]$$

Next, we vary the $\tilde{E}$ and K values, and we choose the model which minimizes the chi-squared as the best model to represent the data (16). The chi-squared value is calculated according to:

$$\chi^2(K,\tilde{E}) = \frac{1}{N-2-1}\sum_{i=1}^{N\ data\ points}\left(\frac{E_{app,theory,i} - E_{app,i}}{\sigma_i}\right)^2 \quad [S7]$$

We followed the same basic procedure for fitting of higher order oligomerization models, except that there was no proximity FRET correction: $E_{app} \approx E_{oligo}^{Dq}$. As discussed above, this approximation is justified as the stochastic FRET contribution to the signal decreases significantly as a function of oligomer order (18).

To record the fraction of oligomers as a function of total concentration and an equilibrium association constant for the association of n monomers to an n'th order oligomer, $n * [m] \rightleftharpoons oligo$, one must find the roots of an n'th order equation. Instead of finding the analytical solution

for the fraction of oligomers as a function of total receptor concentration, which is impossible for n > 5, we utilized a MATLAB root finding function to numerically calculate the roots of the binding polynomial. We took the largest real root as the physical solution to the n'th order polynomial which yields [m_i] as a function of K_A and [T_i]. As with the case of the monomer-dimer equilibrium, we varied the $\tilde{E}$ and K values, and we chose the model which minimized the chi-squared as the best-fit model to represent the data (Eq. S7).

Having determined the association constants of oligomerization for β_2AR ($8.3 \pm 0.9 \times 10^2$ dimer/receptor^2) and for CB_1 ($2.0 \pm 1.0 \times 10^{11}$ tetramer/receptor^4), we could then calculate the apparent Gibbs free energy of association (ΔG_a) by:

$$\Delta G_a = -RTln(K_a) \quad [S8]$$

where R is the universal gas constant, and T is temperature in Kelvin (T = 293±14 K).

1.13 Estimation of β_2AR association energies as a function of membrane curvature

Previously (6), we determined the standard Gibbs free energy of association to be -4.66 ± 0.24 kcal/mole (-8 k_BT) for proteoliposomes of 120 – 130 nm in diameter. In this study we utilized a theoretical scheme (17) that describes the FRET efficiency of dimerizing receptors in a 2D membrane environment based on two contributions: a) the efficiency arising from random collisions and b) the efficiency arising from dimerized proteins. An analytical approximation of the FRET efficiency for a random distribution of donors and acceptors in a 2D membrane is given by (17)

$$E_{Random} = 1 - (A_1 e^{-k_1 C_a} + A_2 e^{-k_2 C_a}) \quad [S9]$$

Here the concept of reduced acceptor density (C_a) is introduced as the acceptor surface density multiplied by a Förster radius (R_0) area (R_0^2)(For Cy3/Cy5 R_0=53 Å (19)). $A_{1,2}$ and $k_{1,2}$ are constants that vary for different values of (R_e/R_0), R_e being the closest approach between donor and acceptor when attached to receptors. Based on structural information R_e/R_0 was assumed to be 1 (20) for reconstituted β_2AR. For a system including dimerized donors and acceptors, the FRET efficiency is given by

$$E_{FRET} = (1 - f_b)E_{Random} + f_b E_{Bound} \quad [S10]$$

where E_{bound} is the FRET efficiency within a dimer. E_{bound} is weighted by the fraction of bound donors (f_b), as the probability that a randomly chosen donor is bound to an acceptor. f_b can be expressed as the probability that a single randomly chosen donor will be in a dimer (f_d) multiplied by the probability that the second unit in the dimer is an acceptor (P_A) (21). P_A is expressed in terms of reduced donor and acceptor densities as $C_a/(C_a+C_d)$.

$$E_{FRET} = (1 - f_d P_A)E_{Random} + f_d P_A E_{Bound} \quad [S11]$$

The fraction of dimers can thus be expressed as

$$f_d = \left(\frac{E_{FRET} - E_{Random}}{E_{bound} - E_{Random}}\right)\frac{1}{P_A} \quad [S12]$$

Because both acceptor density and total receptor density is constant in the analysis performed here (see **Fig. S3 *D***), E_{random} and P_A are constant. Assuming that E_{bound} remains unchanged with curvature, and utilizing the E_{bound} obtained for β_2AR (~0.2), we can therefore calculate the fraction of dimers for each curvature, employing the measured E_{FRET} (**Fig. 3 *A***).

For a monomer dimer equilibrium, $[M] + [M] \leftrightarrow [D]$, the association constant is given by

$$K_a = \frac{[D]}{[M]^2} \quad [S13]$$

As pointed out by Fleming *et al* (22) it is crucial for a correct thermodynamic description of protein association in a hydrophobic solute to apply the effective concentration of proteins in the lipid phase. This is in contrast to, for example, protein concentration in the total volume of buffer and lipids. In accordance with this we employed the mole fraction scale, permitting extraction of a standard Gibbs free energy that can be directly compared to reported literature values. The fraction of dimers can be expressed in terms of K_a and the total receptor mole fraction X_p according to (23)

$$f_d = \frac{4K_aX_p + 1 - \sqrt{8K_aX_p + 1}}{4K_aX_p} \quad [S14]$$

where (X_p) is given by

$$X_P = \frac{2N_{protein}}{2N_{protein} + N_{lipids}} = \frac{2N_{protein}}{2N_{protein} + 2\frac{A_{liposome}}{A_{lipid}}} \quad [S15]$$

$N_{protein}$ and N_{lipids} being the numbers of receptors and lipids respectively and two accounting for the transmembrane nature of the receptors. Due to the lipid bilayer N_{lipids} is given by twice the liposome area ($A_{liposome}$) divided by the lipid headgroup area (A_{lipid}= 0.67 nm^2) (24).

Isolating K_a in Eq. S16 yields a solution given by

$$K_a = \frac{f_d}{2X_p(f_d - 1)^2} \quad [S16]$$

Hence, from the calculated fraction of dimers we obtain a K_a at the molefraction scale for each curvature, and finally a standard Gibbs free association energy according to Eq. S8. K_a obtained on the molefraction scale is converted to units of copies/Area according to the scheme published by Provasi *et al.* (25) using a lipid headgroup area of 0.67 nm^2 (24).

1.14 Calculation of β_2AR on-rates

A prototypical model for diffusion of cylindrical inclusions in membranes is the Saffman-Delbrück model (26), which treats the membrane as a 2D viscous fluid with two dimensional viscosity $\eta_m = h\nu_m$, h being thickness and ν_m the lipid viscosity, surrounded by a 3D ("embedding") fluid with three dimensional viscosity ν_w. The diffusion of a cylindrical inclusion of radius a is given by $D_{SD} = D_0 / 4\pi\ (\ln(2\xi_0/a_c) - \gamma)$, where a_c is the protomer radius, γ the Euler-Mascheroni constant, $D_0 = k_BT/\eta_m \sim 10$ nm^2/μs sets the units for the diffusion constant and $\xi_0 = \eta_m/(2\nu_w)$ is the Saffman-Delbrück length, i.e. the characteristic scale beyond which the membrane exchanges in-plane momentum with the surrounding fluid. This model is derived from hydrodynamic considerations for the 2D flat slab surrounded by the embedding solvent. Using ν_w ~1cP and ν_m~1P gives ξ_0=200 nm.

Generalizing this to the spherical case (27), the co-rotational diffusion of the inclusion of particles in liposomes – that is the mobility of the proteins with respect to the vesicle – is given by:

$$D_{co-rot} = \frac{D_0}{8\pi} \sum_{l=2}^{l_{max}} \frac{2l+1}{s_l} \quad [S17]$$

$s_l = l(l+1) - 2 + 2R/\xi_0\ (2l+1)$, R being the vesicle radius.The cutoff $l_{max} = \exp(-\gamma)\ 2R/a_c$ was introduced to regularize a high-momentum divergence and was chosen so that the for vanishing

curvature, Eq. S15 gives the flat Saffman-Delbrück result. The diffusion for proteins (a_c ~ 3.0 nm) in vesicles of different diameters estimated with Eq. S17 are plotted in **Fig. 3** ***D***. To convert this diffusion into a dimerization rate, we assumed a diffusion-limited dimerization step, and used the Smoulchowski theory in 2D to obtain the on-rate k_{on}

$$k_{on}(D_c) = \frac{4\pi D_c}{\ln\left(\frac{4\pi D_c t_{exp}}{a_c^2}\right) - \gamma} \quad [S18]$$

where t_{exp} refers to typical experimental time scales explored to detect diffusion, and D_c is the diffusion constant of the protomers. Combined, Eq. S17 and Eq. S18 allowed us to calculate the on-rate as a function of the membrane curvature (see **Fig. 3** ***D***).

2 SUPPORTING FIGURES AND TABLES

2.1 Supporting Figure 1

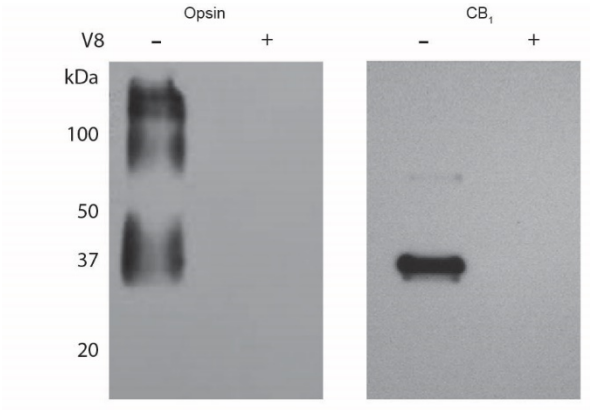

Orientation of CB1 and opsin in proteoliposomes. To assess the orientation of the receptor in proteoliposomes, we tested proteoliposome samples for their susceptibility to proteolysis by V8 protease. The V8 protease can cleave opsin and our CB1 purification mutant at the C-terminus, causing a loss of the 1D4 epitope. For digestion to occur the cytoplasmic face must be exposed (i.e. on the outside of the vesicles). Immunoblot analysis with an anti C-terminal antibody (1D4, that binds to both opsin and our CB1 purification mutant) showed that liposome samples incubated with V8 protease (+) show a loss of epitope binding compared to samples without V8 protease incubation (-). The immunoblot in **Fig. S1** reveals that the vast majority of CB1 and opsin samples are oriented inside-out.

2.2 Supporting Figure 2

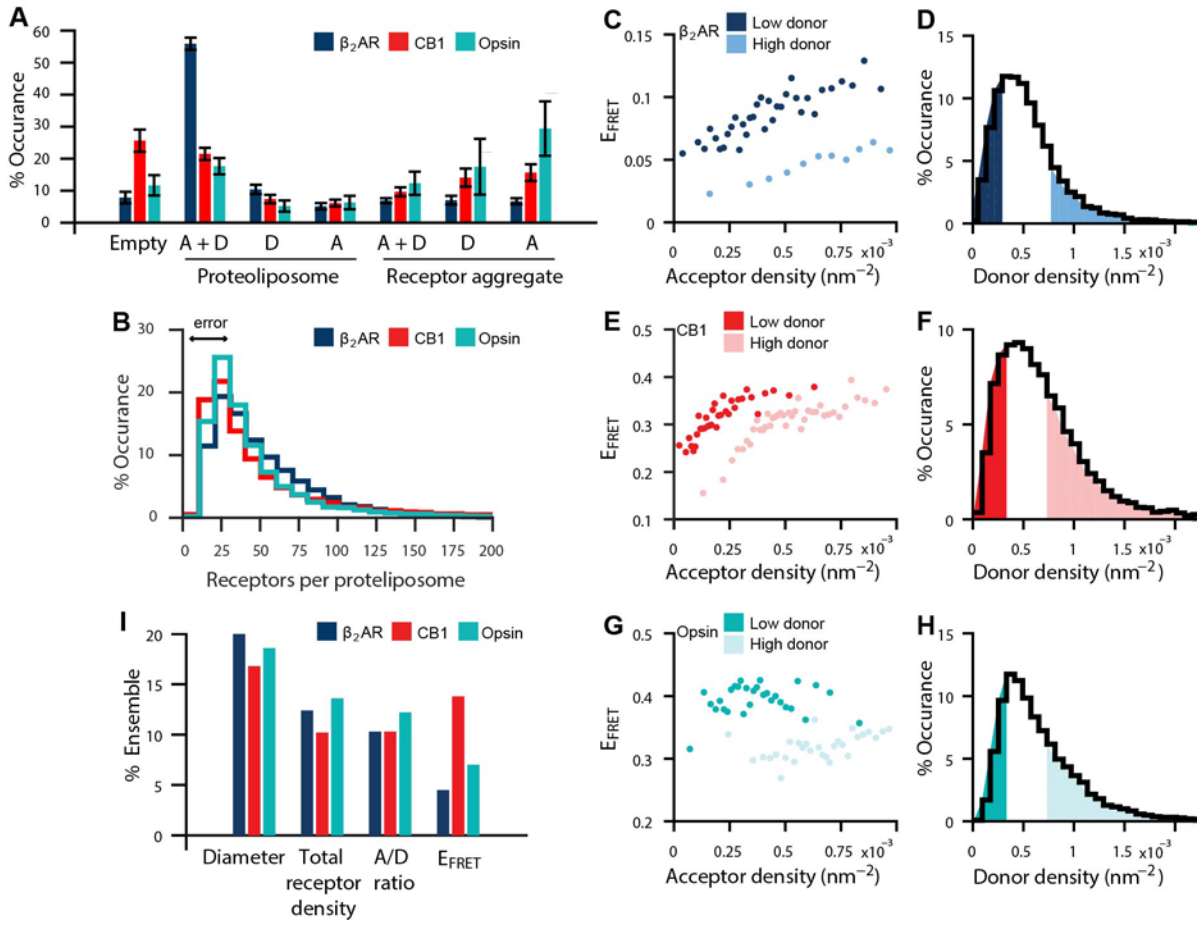

Characterization of proteoliposome samples. (**A**) Particle subpopulations within GPCR reconstituted proteoliposome samples included empty proteoliposomes (Empty), proteoliposomes with both donor and acceptor (A+D), only donors GPCR (D) and only acceptors (A) labeled GPCRs, and receptor aggregates of only donor (D), only acceptors (A), and donor and acceptor (A+D) labeled GPCRs. For each GPCR the total number of single particles included in the analysis comprises n > 9000 single particles. Data is shown as a weighted average with uncertainties representing the standard deviation of technical replicates from 3 independent experiments. (**B**) Histogram displaying of the number of receptors in individual (A+D) proteoliposomes. For each GPCR data comprise n > 12800 single proteoliposomes from > 5 technical replicates. Error shown represents the full width of the propagated error histogram for the GPCR with the largest error. (**C-H**) E_{FRET} is specific and not due to stochastic interactions. (**C, E, G**) We plot E_{FRET} as a function of total acceptor density at a low ($0 – 0.3 \times 10^{-3}$ receptors/nm^2) and high ($0.8 – 10 \times 10^{-3}$ receptors/nm^2) total donor density. Because we see a relative increase of E_{FRET} at lower total density of donor we conclude that FRET is a result of specific interaction of GPCR monomers and is not due to by-stander FRET (28). Data in **C, E, G** were binned (100 single proteoliposomes per bin) and a weighted average shown. For each GPCR and each donor density selection (low or high) data n > 1100 single proteoliposomes. Uncertainties are less than or equal to the displayed marker size. Proteoliposomes selected for analysis in **C, E, G** are shown in panels (**D, F, H**) as a histogram of total donor density. (**I**) To determine how representative ensemble averages were of the underlying single proteoliposome population, we counted the number of single proteoliposomes which fell within the ensemble average ± 10%. Data are shown as a percentage of the total number of single proteoliposomes (see **Table S1**). **Fig. S2** shows that (1) proteoliposome reconstitutions contain significant percentage of unintended particles, (2) E_{FRET} is specific in selected proteoliposomes and is not dominated by

bystander FRET, (3) ensemble proteoliposome measurements do not represent the underlying single proteoliposome population.

2.3 Supporting Figure 3

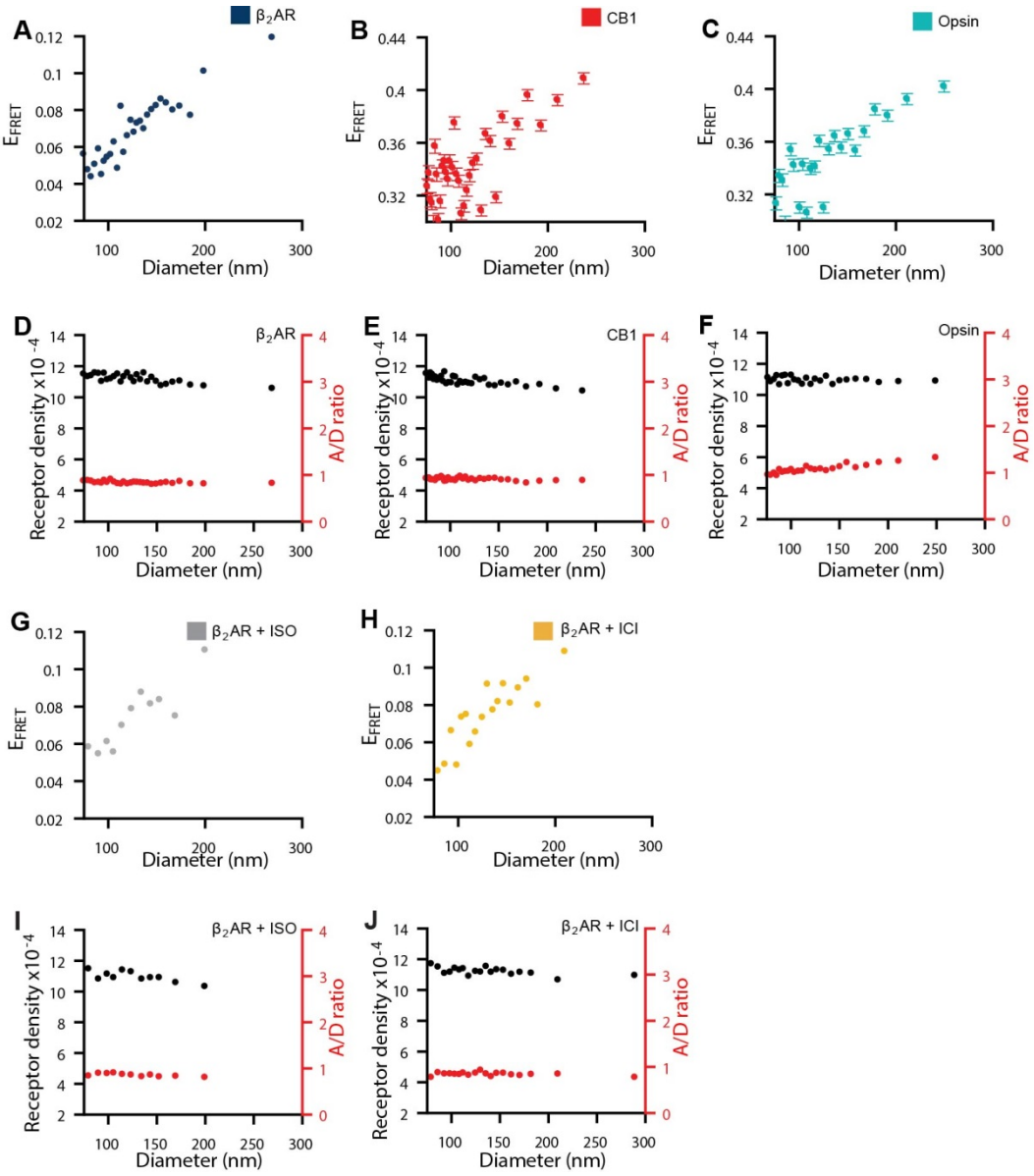

Membrane curvature reduces the oligomerization of GPCRs. (**A-C**) GPCR oligomerization increases as proteoliposome diameter (and planarity) increases. Data in **A-C** were selected for constant donor and acceptor GPCR densities ($0.4 - 0.8 \times 10^{-3}$ receptors/nm^2) and were binned (75 proteoliposomes per bin) with weighted average shown. Data in **A-C** comprise n > 1800 single proteoliposomes. (**D-F**) Controls showing that neither total receptor density (black) nor the A/D ratio (red) vary with proteoliposome diameter. (**G-H**) Response of β_2AR to the agonist Isoproterenol (ISO) or the inverse agonist ICI 118,551 (ICI) at saturating conditions. Ligands do not modify the response of β_2AR to

membrane curvature. Data in **G-H** were selected for constant donor and acceptor GPCR densities ($0.4 - 0.8 \times 10^{-3}$ receptors/nm^2) and were binned (75 proteoliposomes per bin) with a weighted average shown. Data in **G-H** comprise n = 1575 (β_2AR + ICI) or n = 975 (β_2AR + ISO) single proteoliposomes. (**I-J**) Controls showing that neither total receptor density (black) nor the A/D ratio (red) vary with liposome diameter. Uncertainties represent the standard error of the mean and are shown in **B-C** where the uncertainties were larger than the marker size; all other uncertainties are equal to or smaller than marker size shown. Data in **A, G, H** are re-plotted from **Fig. 4** ***A***. **Fig. S3** shows that high membrane curvature decreases GPCR oligomerization.

2.4 Supporting Figure 4

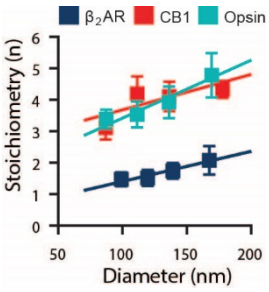

Membrane curvature decreases oligomer stoichiometry. Stoichiometry analysis repeated as in **Fig. 2** ***A*** for proteoliposomes with defined proteoliposome diameters, while maintaining a constant receptor density within $\pm 0.2 \times 10^{-3}$ receptors/nm^2 of the mean (see **Table S1**). The average stoichiometry from each diameter selection is shown. For each GPCR data comprises n > 2500 single proteoliposomes where uncertainties represent ± 1 standard deviation calculated from the fit of Eq. S3. A linear fit to each data set is included to aid interpretation. Data for β_2AR are re-plotted from **Fig. 3** ***B***. **Fig. S4** shows that the stoichiometry decreases in proteoliposomes of low diameters, hence high membrane curvatures.

2.5 Supporting Table 1

		Ensemble	Single Proteoliposome			% Ensemble
Variable	Sample		Mean	STDEV	SEM	
Proteoliposome diameter	β_2AR	101.1	114.5	45.9	0.4	20.0
	CB_1	90.6	125.5	63.0	0.5	16.8
	Opsin	81.8	105.5	48.0	0.4	18.6
Total receptor density (nm^{-2})	β_2AR	1.71×10^{-3}	1.26×10^{-3}	0.8×10^{-3}	0.7×10^{-5}	12.4
	CB_1	1.71×10^{-3}	1.11×10^{-3}	0.8×10^{-3}	0.6×10^{-5}	10.2
	Opsin	1.71×10^{-3}	1.29×10^{-3}	0.7×10^{-3}	0.6×10^{-5}	13.6
A/D Ratio	β_2AR	1.0	1.99	1.79	0.02000	10.3
	CB_1	1.0	0.82	0.54	0.00004	10.3
	Opsin	1.0	1.24	0.76	0.00600	12.2
E_{FRET}	β_2AR	0.27	0.13	0.14	0.001	4.5
	CB_1	0.27	0.34	0.15	0.001	13.8
	Opsin	0.22	0.37	0.16	0.001	7.0

Characterization of proteoliposomes using bulk or single particle approaches. Ensemble measurements or estimates were determined from starting preparation constituents or from averaging all reconstitutional particles. Briefly, ensemble average proteoliposome diameters were determined by averaging the size of all proteoliposomes with and without reconstituted receptor from the single proteoliposome assay. Ensemble average total receptor density (nm^{-2}) were estimated from a 1:1000 receptor to lipid ratio, assuming no lipid or receptor loss, and a lipid head group area of 0.67 nm^2. Ensemble average A- to D-labeled GPCRs (A/D ratio) were estimated from a 1:1 stoichiometry during receptor reconstitution. Ensemble E_{FRET} was determined by summing all fluorescent intensity signals (Methods). Single proteoliposome data represent the means, standard deviations (STDEV), and standard error of the means (SEM) from histograms presented in **Fig. 1** ***D-G*** fit with either a lognormal (total receptor density (nm^{-2}), A/D ratio, and proteoliposome diameter) or normal (E_{FRET}) distributions. The % ensemble represents the percentage of single proteoliposomes for each GPCR having values within ± 10% of the mean predicted by the bulk data. We chose 10% as a reasonable error on the bulk data based on previous reports of RET oligomerization measurements of GPCRs in proteoliposomes (1) and live cells (29).

3 SUPPORTING REFRENCES

1. Fung, J. J., X. Deupi, L. Pardo, X. J. Yao, G. A. Velez-Ruiz, B. T. DeVree, R. K. Sunahara, and B. K. Kobilka. 2009. Ligand-regulated oligomerization of β2-adrenoceptors in a model lipid bilayer. EMBO J. 28:3315-3328.
2. Fay, J. F., T. D. Dunham, and D. L. Farrens. 2005. Cysteine residues in the human cannabinoid receptor: only C257 and C264 are required for a functional receptor, and steric bulk at C386 impairs antagonist SR141716A binding. Biochemistry 44:8757-8769.
3. Ridge, K. D., Z. Lu, X. Liu, and H. G. Khorana. 1995. Structure and function in rhodopsin. Separation and characterization of the correctly folded and misfolded opsins produced

on expression of an opsin mutant gene containing only the native intradiscal cysteine codons. Biochemistry 34:3261-3267.
4. Xie, G., A. K. Gross, and D. D. Oprian. 2003. An opsin mutant with increased thermal stability. Biochemistry 42:1995-2001.
5. Fay, J. F., and D. L. Farrens. 2012. A key agonist-induced conformational change in the cannabinoid receptor CB1 is blocked by the allosteric ligand Org 27569. J. Biol. Chem. 287:33873-33882.
6. Mathiasen, S., S. M. Christensen, J. J. Fung, S. G. Rasmussen, J. F. Fay, S. K. Jorgensen, S. Veshaguri, D. L. Farrens, M. Kiskowski, and B. Kobilka. 2014. Nanoscale high-content analysis using compositional heterogeneities of single proteoliposomes. Nat. Methods 11:931-934.
7. Periasamy, A., H. Wallrabe, Y. Chen, and M. Barroso. 2008. Quantitation of protein–protein interactions: confocal FRET microscopy. Method Cell Biol. 89:569-598.
8. McCann, J. J., U. B. Choi, L. Zheng, K. Weninger, and M. E. Bowen. 2010. Optimizing methods to recover absolute FRET efficiency from immobilized single molecules. Biophys. J. 99:961-970.
9. Bendix, P. M., M. S. Pedersen, and D. Stamou. 2009. Quantification of nano-scale intermembrane contact areas by using fluorescence resonance energy transfer. Proc. Natl. Acad. Sci. U.S.A. 106:12341-12346.
10. Kunding, A. H., M. W. Mortensen, S. M. Christensen, and D. Stamou. 2008. A fluorescence-based technique to construct size distributions from single-object measurements: application to the extrusion of lipid vesicles. Biophys. J. 95:1176-1188.
11. Ulbrich, M. H., and E. Y. Isacoff. 2007. Subunit counting in membrane-bound proteins. Nature methods 4:319-321.
12. Veatch, W., and L. Stryer. 1977. The dimeric nature of the gramicidin A transmembrane channel: conductance and fluorescence energy transfer studies of hybrid channels. J. Mol. Biol. 113:89-102.
13. James, J. R., M. I. Oliveira, A. M. Carmo, A. Iaboni, and S. J. Davis. 2006. A rigorous experimental framework for detecting protein oligomerization using bioluminescence resonance energy transfer. Nat. Methods 3:1001-1006.
14. Raicu, V. 2007. Efficiency of resonance energy transfer in homo-oligomeric complexes of proteins. J. Biol. Phys. 33:109-127.
15. Patowary, S., L. F. Pisterzi, G. Biener, J. D. Holz, J. A. Oliver, J. W. Wells, and V. Raicu. 2015. Experimental Verification of the Kinetic Theory of FRET Using Optical Microspectroscopy and Obligate Oligomers. Biophys. J. 108:1613-1622.
16. Press, W. H., Flannery, B. P. , Teukolsky, S. A. , Vetterling, W. T. . 1989. Numerical Recipies. The Art of Scientific Computing. Cambridge University Press, Cambridge.
17. Wolber, P., and B. Hudson. 1979. An analytic solution to the Förster energy transfer problem in two dimensions. Biophys. J. 28:197-210.
18. King, C., S. Sarabipour, P. Byrne, D. J. Leahy, and K. Hristova. 2014. The FRET signatures of noninteracting proteins in membranes: simulations and experiments. Biophys. J. 106:1309-1317.
19. Mansoor, S. E., K. Palczewski, and D. L. Farrens. 2006. Rhodopsin self-associates in asolectin liposomes. Proc. Natl. Acad. Sci. U.S.A. 103:3060-3065.

20. Kenworthy, A., and M. Edidin. 1998. Distribution of a glycosylphosphatidylinositol-anchored protein at the apical surface of MDCK cells examined at a resolution of< 100 Å using imaging fluorescence resonance energy transfer. J. Cell Biol. 142:69-84.
21. Adair, B. D., and D. M. Engelman. 1994. Glycophorin A helical transmembrane domains dimerize in phospholipid bilayers: a resonance energy transfer study. Biochemistry 33:5539-5544.
22. Fleming, K. G. 2002. Standardizing the free energy change of transmembrane helix–helix interactions. J. Mol. Biol. 323:563–571.
23. Yano, Y., and K. Matsuzaki. 2006. Measurement of thermodynamic parameters for hydrophobic mismatch 1: self-association of a transmembrane helix. Biochemistry 45:3370-3378.
24. Marrink, S. J., A. H. De Vries, and A. E. Mark. 2004. Coarse grained model for semiquantitative lipid simulations. J. Phys. Chem. B: Cond. Phase 108:750-760.
25. Provasi, D., J. M. Johnston, and M. Filizola. 2010. Lessons from free energy simulations of δ-opioid receptor homodimers involving the fourth transmembrane helix. Biochemistry 49:6771-6776.
26. Saffman, P., and M. Delbrück. 1975. Brownian motion in biological membranes. Proc. Natl. Acad. Sci. U.S.A. 72:3111-3113.
27. Henle, M. L., and A. J. Levine. 2010. Hydrodynamics in curved membranes: The effect of geometry on particulate mobility. Phys. Rev. E 81:011905.
28. Lan, T.-H., Q. Liu, C. Li, G. Wu, J. Steyaert, and N. A. Lambert. 2015. BRET evidence that β2 adrenergic receptors do not oligomerize in cells. Sci. Rep. 5:doi:10.1038/srep10166.
29. Mercier, J.-F., A. Salahpour, S. Angers, A. Breit, and M. Bouvier. 2002. Quantitative assessment of β1-and β2-adrenergic receptor homo-and heterodimerization by bioluminescence resonance energy transfer. J. Biol. Chem. 277:44925-44931.